ELSEVIER

Spectrochimica Acta Part B 55 (2000) 1195–1240

SPECTROCHIMICA ACTA PART B

www.elsevier.nl/locate/sab

Review

Axially and radially viewed inductively coupled plasmas — a critical review

I.B. Brenner*[,1], A.T. Zander[2]

Varian, Inc., 3120 Hansen Way, Palo Alto, CA 94304, USA

Received 16 February 1999; accepted 19 May 2000

Abstract

The present status of axially viewed inductively coupled plasmas (ICP) is reviewed with special emphasis placed on the analytical performance of currently available systems. Descriptions are given of the various designs of the plasma–spectrometer configuration. Conventional figures of merit such as limits of detection, background behavior, interferences due to easily ionized elements (EIE), Ca and acids, and the Mg II 280.270 nm/Mg I 285.213 nm intensity ratio, are used to compare the performance of axially viewed and radially viewed ICPs. Various modes of sample introduction, including conventional pneumatic and ultrasonic nebulization (USN), thermospray and a direct injection probe will be described. For axially viewed ICPs, limits of detection (LOD) are improved by factors varying from approximately 2 to 30. Additional improvements by factors of 2–20 can be obtained using USN. The improvement factors generally depend on energy potentials of the spectral lines and the element. Although limits of detection in the presence of Ca and Na are degraded relative to an aqueous solution 10–30-fold, USN LODs using an axially viewed ICP are improved relative to those obtained using a pneumatic nebulizer for solutions containing Ca and Na. With normal aerosol load and under robust plasma conditions (as evidenced by Mg II/Mg I intensity ratios >8), EIE, Ca and mineral acid induced interferences are relatively small and are similar in axial and conventional radial configurations. However, interferences due to Ca are larger than those caused by Na due to the larger amount of energy required to dissociate the matrix. Matrix effects increase considerably when an USN is employed. For robust plasmas, ICP operating conditions and performance for multi-element quantitative analysis do not differ significantly from those of conventional radial configurations. In cases where robustness decreases, matrix interferences should be taken into account when establishing optimum conditions for operation. In robust axially viewed ICPs, a single internal standard can compensate for ionic line intensity suppression due to Na. However,

* Corresponding author. Fax: +972-2-6797-145.

E-mail address: brenner@cc.huji.ac.il (I.B. Brenner).

[1] Present address: Environmental Analytical Laboratory, Ben Gurion University of the Negev. 9 Dishon Street, Malkha, Jerusalem 96956, Israel.

[2] Present address: Molecular Devices, Inc., 1311 Orleans Drive, Sunnyvale, CA 94089, USA.

0584-8547/00/$ - see front matter
PII: S0584-8547(00)00243-3

owing to the variable influence of Ca on spectral response, more than one internal standard is required to compensate for these matrix effects. In this situation, linear energy potential-interference functions can be used to improve accuracy using spectral lines varying over wide ranges of energy potentials. In axially viewed ICPs, Mg II/Mg I ratios vary widely as a function of applied RF power, aerosol flow rates and load, diameter of the central torch injector, and composition of the aspirated solution. The highest values of 9–13 have been observed for a pure aqueous solution using conventional nebulization and argon carrier flow rates (0.5–0.7 ml min^{-1}) and forward powers of 1.2–1.5 kW. Mg II/Mg I ratios decrease when the RF power decreases, when Na and Ca are added to the plasma, and when the aerosol load is increased. A low value of 2 was obtained when the carrier gas flow rate was high and when the aerosol load was high using an USN. The use of a copper metal skimmer below the analytical observation zone to isolate the axial channel of the ICP and to deflect the outer cool fringe results in 5–20 times improvement of the LODs compared to those obtained using a conventional configuration (a normal radially viewed ICP). A direct He purged plasma–spectrometer interface for end-on detection of the vacuum UV (VUV) emission from the axial region of an ICP allows the determination of Cl, Br and other analytes in the $\mu g\ l^{-1}$ range. The characteristics of a secondary discharge at the orifice of a Cu cone when the axial channel of the ICP is extracted into a vacuum chamber will be discussed. The characteristics of the emission in the Mach disk region extracted from the axial column will be surveyed. Several applications and techniques are described: determination of major, minor and trace elements in geological, environmental and biological materials, analysis of brines, nuclear materials and organic solvents and solutions. Several unique techniques are described: elemental speciation, determination of the halides and other analytes with VUV spectral lines using a He purged direct plasma–spectrometer interface. Direct solids analysis using slurries, laser and spark ablation and direct solids insertion further extends the scope of axially viewed ICPs.

Keywords: Axial and radial viewing; Limits of detection; Sample introduction; Interference effects; Mg II/Mg I intensity ratio

1. Introduction

An axially or end-on viewed inductively coupled plasma (ICP) as opposed to radially or side-on viewed can be defined as the observation of the plasma from its apex along the plasma column in the direction of the plasma fireball. Until recently, the ICP with atomic emission detection has been routinely viewed radially at 90° to the central channel of the plasma. With this conventional mode of operation the limits of detection (LODs) can be improved by increasing the efficiency of aerosol generation and transport using ultrasonic nebulization (USN) with desolvation [1,2], thermospray [3,4], by analyte preconcentration and matrix elimination [5] and improving the signal-to-background ratio by enhancing spectral resolution [6]. Further signal enhancements have been achieved by using mixed gas Ar plasmas containing hydrogen [7] and by creating a 'pinch' plasma [8]. For low excitation energy elements, LODs can also be improved by increasing the aerosol or the so-called sheath gas flow (an auxiliary gas flow introduced around the aerosol stream between the torch and the spray chamber) [9]. This results in a temperature decrease, which enhances the intensities of low energy potential spectral lines.

Improvement of LODs is a challenge for ICP atomic emission spectrometry (AES), as the abundance of several elements of environmental, biological and geochemical significance is too low for direct determination. In the last few decades, it was shown that ICP-AES LODs could be improved substantially by axial viewing of the plasma [10–22]. The first report on the performance of an axially viewed ICP was by Mermet and co-workers in 1976 [10]. In that publication, the setup both for AES and atomic absorption spectrometry (AAS) measurements was described. LODs were improved up to fivefold; the linear range was approximately four orders of magnitude. Lichte and Koirtyohann [11], Demers [12], Kornblum [13], Danielsson (in Kornblum [13]) and Faires et al. [14], among others, compared axial configurations with the conventional radial

observation. Demers [12] reported up to a 10-fold improvement of LODs for an axially viewed ICP. A close inspection of Demer's data reveals that most of the LOD improvement is due to a decrease in the relative standard deviation (R.S.D.) of the background. Signal-to-background ratios (SBR) were not improved by a factor of 10. Indeed, in some cases they even decreased (e.g. Pb II 220.353 nm, Mermet, personal communication). Moreover, the dynamic range was reduced and EIEs and alkali earth elements affected the spectral response. The decrease in dynamic range was attributed to cool absorbing atoms along the optical viewing path, while matrix interferences were attributed to the observation of solution vaporization and ionization effects in the cool plasma fringe. In the second ICP Conference in Noordwijk aan Zee in 1978, Danielsson (in Kornblum [13]) reported data on the performance of an ICP using an intensified diode array emission spectrometer (IDES) detector. It was observed that the SBRs of both the atom and the ion lines have maximum values in the central part of the plasma column and that they were higher than those of radially viewed ICPs by up to an order of magnitude. Argon lines and background continuum showed maximum intensities in the 'skin zone'. It was also observed that the maximum intensities of As, Ge, Sb, and C were off axis and that they were dependent on the flow rate and RF power. Demers [12] and De Loos-Vollebregt et al. [16] employed a water-cooled low-power ICP and found in contradiction to the results previously cited, that compared to a conventional plasma the linearity of the calibration curves of their axially viewed system was the same. Moreover, there was a remarkable reduction of interferences. Fuxing et al. [17,18] used an axially viewed ICP coupled to a quartz prism emission spectrograph for the determinations of trace elements in NaCl brines.

Montaser and Fassel [23] located a copper metal skimmer below the analytical observation zone to isolate the axial channel of the ICP and to deflect the outer cool fringe. They observed that SBRs and LODs were 5–20 times superior to those obtained using a conventional configuration. In the late 1980s, Houk and his co-workers [24–27], reported both fundamental and analytical investigations of the VUV emission from the axial region of an atmospheric pressure ICP using a unique direct plasma–spectrometer interface. A water-cooled Cu-metal cone with a circular orifice was mounted on the entrance slit of a He-purged monochromator. The VUV spectral lines of Cl, Br and other analytes were observed, showing μg l^{-1} LODs. Houk and his co-workers [24–27] described the characteristics of a secondary discharge generated on the tip of a Cu-metal cone, when the axial channel of the ICP was extracted into a vacuum chamber. The intensities of the ion lines were enhanced by an order of magnitude relative to the ICP itself. However, the low energy potential atom lines were suppressed. This secondary discharge, which sampled the axial region of the ICP, was claimed to have analytical benefits for AES. It was concluded that atomization, excitation and ionization processes prevailing in this axial discharge are more efficient than in the plasma itself. Indeed, a similar discharge was employed to vaporize solid samples for introduction into the ICP by Farnsworth and Hieftje [28].

Lim and Houk [29] were first to report measurements of optical emission spectra in reduced-pressure plasmas extracted from the axial region of an atmospheric ICP. In comparison to a conventional ICP, the analyte intensities from the reduced pressure discharge were lower by factors up to 1000. Borer and Hiefjte [30,31] also evaluated an axially viewed microwave-boosted reduced-pressure plasma extracted from an atmospheric ICP. Luan et al. [32] and Ma'an and Houk [33] described the characteristics of the emission in the Mach disk region generated from the axial column of a 40-MHz ICP. Intensities in the Mach disk were lower than those observed in conventional radially and axially viewed ICPs by factors varying from 100 to 1000.

The development of axially viewed ICPs in commercially available instrumentation is among the most important event since the introduction of the ICP in 1969 as a competitive atomization and excitation source for single and multi-element analysis. Surprisingly, instrument vendors did not recognize the analytical advantages of this

simple arrangement until the early 1990s. This was due to the conflicting reports describing the response of axially viewed ICPs to various interference effects, with detailed characterizations being neglected. Recently however, the strengths and weaknesses of axially viewed plasmas were reconsidered in response to the challenge to improve LODs for environmental analysis using ICP-AES. A period of intense study aimed at examining the analytical advantages and disadvantages of this configuration resulted in an increase in the number of publications and the availability of commercial instrumentation. Perusal of the recent literature [34–44] indicates that emphasis has been placed on the comparison of the axial configurations with radially observed ICPs. The studies focus mainly on LOD improvements and EIE, Ca and mineral acid interferences on the emission signals of ion and atom lines using conventional and high aerosol loads, and the role of internal standardization. Claims are now being made that the analytical performance of axially viewed robust ICPs is similar to that obtained with radial viewing [35,36,40–44].

This review is undertaken with this consideration in mind and an attempt will be made to provide answers to the following issues: is the analytical performance of axially viewed ICPs similar to radially viewed configurations, and what are the limitations and benefits? The review will cover the following topics: instrumentation, analytical figures of merit such as LODs, the magnitude and nature of interferences due to EIEs, Ca, and mineral acids; influence of ICP operating conditions such as RF power and aerosol flow rate. The relation with energy potentials of the analyte lines will be outlined. The utility of the Mg II 280.270 nm/Mg I 285.213 intensity ratio as a criterion of plasma robustness will be examined. Several applications will be described: geological, biological and agricultural samples, foods, cosmetics, steels, analysis of organic solvents, solutions, speciation, determination of the halides using VUV spectral lines, and direct solids analysis using slurry nebulization, laser and spark ablation, and direct solids insertion.

2. Instrumentation

2.1. Torch configuration

In axially viewed ICPs the configuration of the torch itself is somewhat different from those used in radial viewing. Abdallah et al. [10] used an adjustable demountable torch, the outer sleeve of

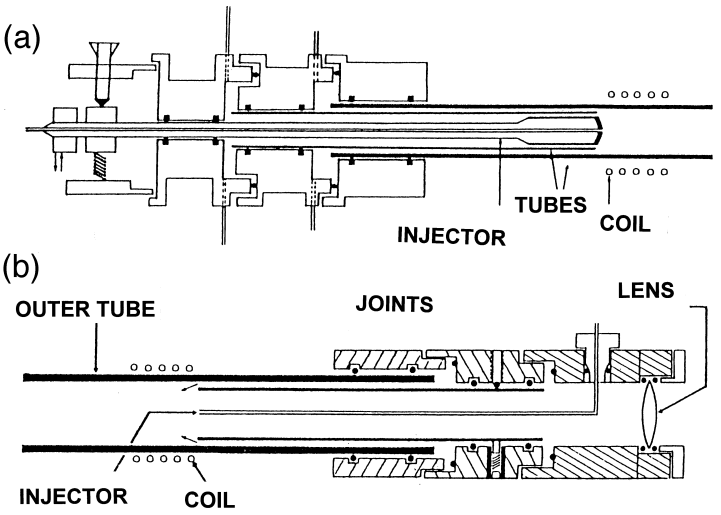

Fig. 1. Adjustable demountable torch used by Abdallah et al. [10] for axial viewing. (a) Torch for atomic emission detection; (b) assembly for atomic absorption spectrometry.

which was extended (Fig. 1). The number of turns in the RF coil was five. In axially viewed ICPs, the outer sleeve of the torch is now commonly extended so that the plasma is confined and air entrainment is minimized. Nakamura et al. [39,45] studied the analytical performance of a long torch. LODs of 24 elements in the spectral range 210–770 nm were measured and it was observed that they were improved from 50% for Be to sevenfold for Al. In the configuration used by Brenner et al. [36] an extended torch with a wide 2.3-mm injector, was positioned in the holder so that the distance between the intermediate tube and the load coil was approximately 2 mm. The distance between the coil and the top of the outer tube of the torch was 3 mm, and the distance between the top of the outer tube of the torch and the cooled cone was 1.4 mm [36]. In the study described by Brenner et al. [37], the viewing position was automatically adjusted using Mn II 257.610 nm. The Mn emission was continuously measured while the X–Y–Z position of the torch was moved under computer control. The top of the torch injector (2 mm i.d.) was positioned 0.25–1 mm below the intermediate tube and the distance of the cut-off gas snout from the top of the plasma coil was 5 mm. De Loos-Vollebregt [4] used a low-flow water-cooled ICP. A ball-shaped plasma, highly suitable for axial viewing, was formed. LODs were improved by a factor of 4. A cut-off gas was not employed. Dalhquist et al. [46], employed a ceramic torch. The use of pure alumina torches has an advantage if low Si levels have to be determined.

Huang et al. [47] investigated matrix effects with an extended torch using laser excited fluorescence and emission. They measured the intensities of Ca I, Ca II, Ba I, Ba II, Mg I, Mg II, Na I and Cu I lines as a function of RF power and observed that the relationships were different from those found with a conventional short ICP torch. The effect of K on the fluorescence of Ca I and Ca II lines was considerably larger than with a conventional short torch. These authors cautioned that the use of extended torches such as those used in axially viewed ICPs could result in substantial ionization interferences.

An important component of the torch is the internal diameter of the central injector. Mermet and co-workers [35,42,43,48–50] showed that residence time and plasma robustness increased when a wide (>2 mm) central torch injector is employed. They emphasized the influence of the torch injector diameter on energy transfer from the plasma to the central channel. Indeed when Ivaldi and Tyson [34] used a narrow bore injector, the Mg II 280.270/Mg I 285.213 intensity ratios were low indicating that the plasma was not robust. Brenner et al. [37] using the same instrument and torch configuration employed a wider injector (2 mm) and obtained higher ratios. Brenner et al. [36] also used a wide central injector (2.3 mm) with a sequential spectrometer (Varian Liberty) and a high efficiency RF power generator, and obtained high Mg II/Mg I ratios (>8) even at 1 kW. Wide injectors up to 3 mm are installed in JY demountable Ryton torches.

Conver et al. [51] evaluated the performance of a fused silica aperture thermospray (FSApT) with axial viewing. The %R.S.D.s for FSApT were similar to pneumatic sample introduction levels, and 10-fold LOD improvements were reported when a narrow torch central injector was employed (see additional discussion in Section 4.1).

2.2. Plasma–spectrometer interface

In axially viewed ICPs, the emission from the excited analytes in the central column of the plasma is isolated from the surrounding argon radiation. The spectrometer is focused on the axial region via transfer lenses or a flat mirror mounted above the vertically oriented plasma [52]. A shear gas flow is used to remove the plasma fringe, minimize self-absorption, protect the optical interface from thermal damage, and prevent salt deposition on the entrance optic lenses and mirrors. Removal of the cool fringe also reduces matrix effects due to EIEs and Ca and extends the linear range of calibration and determination. If the shear gas is N_2 or Ar it also allows determinations in the UV region of the spectrum. The disadvantage of using air as a shear gas is the certainty of air entrainment and the presence of a VUV absorbing medium limiting the spectral

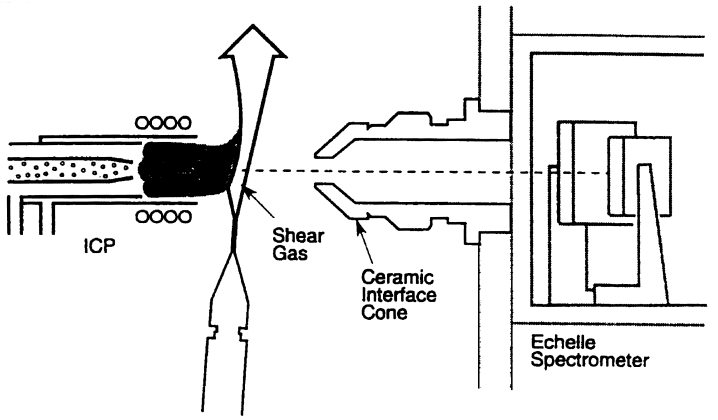

Fig. 2. Schematic axially viewed ICP configuration in the Perkin Elmer Optima 3000, showing the 90° 'shear gas' configuration (with courtesy, Perkin Elmer, Bodensee Werke, Germany).

range to >190 nm. Typical shear gas configurations are illustrated in Figs. 2 and 3. It is evident that two types of configuration are applied-cross flow and end-on.

De Loos-Vollebregt et al. [4,16] evaluated an axially viewed ICP formed in a low-flow water-cooled torch. The plasma discharge was almost spherical, and the tail flame was deflected upwards although a 90° shear gas flow was not employed. Of interest is that these workers reported reduced matrix effects and a linear range of operation that was similar to those of radially viewed ICPs. It seems that these favorable characteristics were due to the deflection of the cold plasma fringe. In commercially available instruments, the prevalent shear gas configuration is 90°. This is the most obvious approach to implement. In both configurations, the mechanism is computer driven for accuracy, the optics are designed to maintain a long depth of focus, and the optimum plasma volume is selected so that the SBR is maximum. Mermet noted (personal communication) that there is a problem of focusing a circular image onto a rectangular slit. In the IRIS^{TM} (Thermo Optek) a circular entrance slit was employed with the axially viewed systems. Nakamura et al. [39] employed a water-cooled Cu metal cone positioned between the ICP and the focal lens.

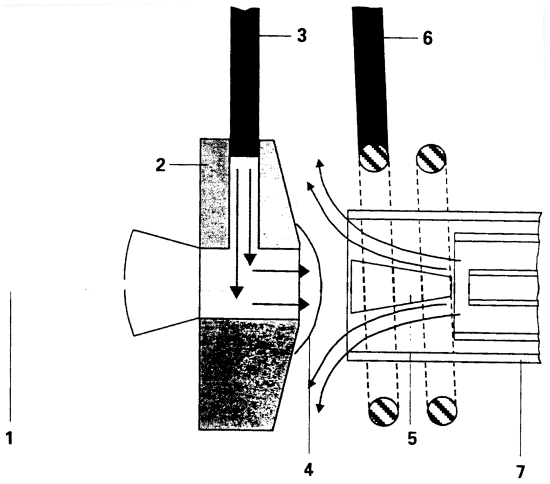

Fig. 3. Schematic illustration of the Spectro EOP axially viewed ICP configuration (Spectro EOP brochure, with courtesy, Spectro, Kleve, Germany). (1) Spectrometer optics, (2) water-cooled plasma interface, (3) argon supply, (4) plume, (5) analytical zone, (6) RF coil, (7) plasma torch.

2.2.1. Cross-flow shear gas

In the cross-flow configuration, the outer fringe of the plasma is diverted from the optical path by a flow of air, N_2 or Ar. Visual inspection of this configuration shows that the plasma is deformed in the area of contact (Fig. 2) and the possibility of turbulence in the impact zone cannot be

excluded. The cross-flow configuration was employed by Fuxing et al. [17,18] with a quartz prism optical emission spectrograph. The cross flow configuration is employed in the Perkin Elmer, Jobin Yvon, TJA Solutions and Leeman axially viewed ICPs.

2.2.2. End-on gas flow

Houk and co-workers [24–27], first described end-on purging of the plasma–spectrometer region, the optical probe and the plasma itself. Helium was used to purge the spectrometer and the Cu-metal optical probe that was immersed in the ICP. These investigators used this configuration to determine the halide elements and other analytes using sensitive VUV spectral lines (see Section 2.2.4). In the commercial versions, the cool plasma fringe, directed to the spectrometer, is stripped away symmetrically from the optical path by an argon or nitrogen sheath gas that flows end-on through a water-cooled interface. This purging leaves the central axial channel isolated from the interfering plasma sheath. In commercial instruments, it is called the cooled cone interface (CCI) (Varian) and the optical plasma interface (OPI) (Spectro). Nakamura et al. [39] employed an end-on Ar shear gas flow that was introduced into the cone and which passed through a nozzle (6 mm i.d.). This protected the spectrometer optics from the high temperature plasma and prevented salt deposition on the entrance optics. In the end-on configuration, the various zones of the plasma as described by Koirtyohann [53], are not deformed. This is in contrast to cross-flow gas configurations where plasma deformation can be distinctly observed. (Perkin Elmer Optima, TJA Solutions: Iris). In all commercial instruments, the depth of focus mostly includes the normal analytical zone (NAZ) as defined by Koirtyohann [53].

Although the end-on configuration would appear to be more favorable due to the stripping of the cool plasma fringe, a critical examination using an identical detector and optimum operating conditions has not been made. Such an evaluation would clarify the question of whether interference effects are related to the mode of diversion of the cool plasma fringe.

2.2.3. Skimmer

Montaser and Fassel [23] located a copper metal skimmer below the analytical observation zone to isolate the axial channel of the ICP and to deflect the outer cool fringe. They observed that SBRs and LODs of 10 atom lines having various excitation energies were 5–20 times superior to those obtained using a conventional configuration.

2.2.4. Direct coupling

Houk at al [24–27] described the investigations of VUV emission from an ICP using a unique direct plasma–spectrometer coupling interface for axial viewing. A water-cooled Cu-metal cone with a circular sampling orifice was mounted in front of the entrance slit of a He-purged monochromator. (He was selected because it is transparent to < 58 nm.) This optical sampler was immersed into the axial channel of the plasma. A He-counter purge gas flowed through the orifice into the plasma forming a well-defined plume (Fig. 4). This gas flow cooled the orifice, deflected the absorbing fringe of the plasma and prevented salt deposition on the cone tip. The grounding of the torch coils was reversed in order to alleviate arcing from the load coil to the sampler. With the use of a solar blind photomultiplier tube (PMT), Ar resonance lines at 104.82 and 106.87 nm and O lines at 104.09 and 104.17 nm were evident. An optical mask restricted the illuminated slit for improved spatial resolution. Ray tracing indicated that the intensities observed were representative of the axial channel.

2.2.5. Secondary 'pinch' discharges

When the axial channel of the ICP is extracted into a small vacuum chamber, a secondary discharge can be generated at an orifice in a water-cooled Cu-metal cone [8,29]. The diameter of the sampling cone was larger than its length to facilitate cooling and to diminish cone orifice erosion by the discharge. In early ICP-mass spectrometry (MS) this secondary discharge caused orifice erosion and production of so-called 'orifice ions' having high ion kinetic energies [54,55]. The secondary discharge appears as a bright funnel of gas streaming into the orifice. When a concentrated Y solution was introduced into the ICP without

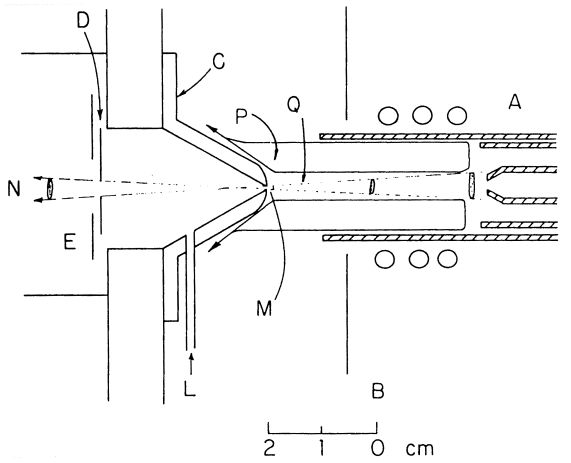

Fig. 4. Schematic reproduction of the direct end-on plasma–spectrometer interface. The water-cooled Cu-metal cone with its sampling orifice is mounted directly on the entrance slit of the He-purged monochromator. Note that the optical sampler is immersed into the axial channel of the plasma. (A) ICP torch and coil, (B) Cu shield, (C) Cu cone with orifice, (D) optical mask, (E) entrance slit, (L) He gas, (M) end-on purge gas flowing into ICP, (N) radiation transmitted to grating, (P) outer plasma fringe. This type of interface was employed by Houk et al. [24–27].

the discharge present, the red emission in the initial radiation zone (IRZ) due to Y I and Y O was present high up in the plasma. This demonstrated that there was insufficient energy in that region of the ICP to generate blue Y II emission. With the discharge, however, blue Y II replaced the red emission of the central axial region [8,29]. This simple experiment demonstrated that the discharge atomized and excited the Y species. The intensities of the ion lines were enhanced by approximately one order of magnitude, whereas the emission signals of low energy potential lines were suppressed.

2.2.6. The Mach disk region

Houk and co-workers [32,33] described studies of the emission in the Mach disk region when the axial region of a 40-MHz ICP was extracted into a small quartz vacuum chamber through a small orifice in a water-cooled Cu plate. The emission was measured with a PE Optima 3000 spectrometer with segmented charge-coupled device detector (SCD). On the ICP side, the sampling cone was shallow to facilitate the sampling of the axial channel. A quartz cylinder was used as the wall of the extraction chamber so that UV emission could be measured. The sampling orifice was positioned 15 mm above the top of the load coil. In the vacuum chamber, a dark 'zone of silence' was surrounded by a concentric shock wave called the 'Mach disk'. Intensities in this region were lower than those observed in a conventional ICP by factors of 100–1000. It is clear that the analytical potential of this configuration is limited unless considerable intensity boosting can be achieved.

2.3. Detection

The radially viewed ICP is the most widely used mode of observation for atomic emission analysis [56–58] that until several years ago was performed mainly with PMT-based polychromators and sequential spectrometers. In the former the sample throughput is high but multi-element coverage is relatively low, whereas in the latter, sample throughput is relatively low, but spectral versatility is high. These shortcomings have been overcome by the advent of charge transfer devices (CTDs) [59–65], which are used to detect radiations dispersed by echelle grating spectrometers. These spectrometers possess the ability to monitor simultaneously a vast number of spectral lines and their spectral backgrounds.

There are several types of commercial CCT configurations used with axially viewed ICPs. The IRIS™ (TJA Solutions, Franklin, MA, USA) charge injection device (CID), described by Denton et al. [59–61], the Optima 3000 XL SCD spectrometer (Perkin Elmer, Norwalk, USA) [62,63] and Varian Vista [64,65] and the Spectro CIROS (Spectro, Kleve, Germany) charge coupled (CCD) spectrometers. In CID and CCD devices, the detectors cover the entire spectral range, whereas in the SCD instrument, segmented arrays have on an average 3–4 primary analytical lines for each of the 72 elements. Perkin Elmer and TJA solutions also manufacture a dual view version (DV) that allows minimization of matrix effects caused by high concentrations of concomitant elements such as Na and Ca. Axial or radial observations can be selected using a periscope

mirror. With the exception of the Spectro CIROS, these instruments are echelle based, whereas the in the CIROS the 22 linear CCD detector arrays are mounted on the Rowland Circle of the Paschen Runge double grating spectrometer.

In the Varian Vista spectrometer, the CCD chip consists of 70 908 pixels that are arranged to match exactly the two-dimensional image from the echelle optics. Almost the entire (96%) spectral range of 167–785 nm is covered. A CaF_2 cross-disperser provides efficient UV transmission. In the Spectro CIROS, the sensitized CCD has access to the very low UV (120 nm) allowing determination of the halogens and other nonmetal elements.

Nakamura and co-workers [39,45] studied the performance of an axially and a radially viewed ICP using a high-dispersion echelle spectrometer. A novel aspect of this instrument was the rapid and automated changeover between radial and axial viewing positions. The reciprocal linear dispersion was 0.031, 0.078 and 0.12 nm mm^{-1} at 200, 500 and 800 nm, respectively. A quartz refractor plate modulated the wavelength sinusoidally and second-derivative detection was obtained by a built-in lock-in amplifier. The system allowed for fine computer controlled adjustment of the plasma torch, both in the horizontal and in the vertical positions. The optimum region of observation was determined based on the maximum signal-to-noise ratios for the analytes studied. Simultaneous background correction was performed.

Axially viewed ICPs have been configured in several PMT-based systems. The Jobin Yvon Panorama system (Jobin Yvon-Horiba, Longjumeau, France) is a conventional 0.5-m Ar-filled Paschen-Runge polychromator. The Ultima (Jobin Yvon-Horiba, Longjumeau, France) is a high-resolution 1-m sequential spectrometer. In Varian Liberty 220 and Series II sequential ICP atomic emission spectrometers, the dispersion system operates in any one of four grating orders of diffraction, and provides an average resolution of approximately 0.009 nm. The Varian Liberty 220 instrument was also used by Conver et al. [51] for the evaluation of a thermospray sample introduction system. The Spectro Spectroflame-EOP (End-On Plasma) is a 0.75-m Ar-filled Paschen Runge polychromator. Dahlquist et al. [46] and Thiel and Danzer [66] described an axially viewed echelle-based ICP spectrometer manufactured by Fisons-called the Maxim (no longer commercially available). This system used optical fiber light guides to transmit the emission to the conventional PMT based spectrometer. PMT outputs were sequentially processed with the aid of a shutter. Oomori et al. [52] recently announced that Shimadzu had developed an axially viewed spectrometer (ICP-7500). The axial view is achieved by observing the vertical plasma using a mirror. Fuxing et al. [17,18] used a quartz prism optical emission spectrograph with a reciprocal linear dispersion varying from 0.35 to 11 nm mm^{-1} and a 27-MHz ICP.

Houk et al. [24–27] used a He-purged monochromator and a direct end-on optical probe for the detection of the VUV spectral lines of the halides and other elements from an axially viewed ICP. A solar blind PMT was used to detect emission down to 106 nm. A scintillation counter was employed for the detection of fluorine < 100 nm. Several commercial instruments (Jobin Yvon, Spectro, TJA Solutions) have the capability of determining the halogens in the VUV (e.g. Cl I 134.724, Br I 157.485, and I I 161.760 nm). The sensitive I 170.207 nm line can also be used by conventional spectrometers.

Interference effects in axially viewed ICPs have been studied using all types of spectrometers [34–38,40,42,45]. Ivaldi and Tyson [34], Dubuisson et al. [40,42], Brenner et al. [37] and Todoli et al. [38] evaluated the Optima 3000 XL in DV mode. Dubuisson et al. [35] and Brenner et al. [36] also compared interference effects of axially and radially viewed ICPs.

3. ICP operating conditions

Mermet and co-workers and other investigators [35–37,40–44,48–50,67–71] showed that robust ICP conditions must be used in order to minimize matrix effects due to EIEs, alkali earths and mineral acids. Such conditions are high RF power (> 1.3 kW), low argon carrier flow rates (< 0.8 l

min^{-1}) and a wide internal diameter of the torch injector. Dalhquist et al. [46] and Coleman [72] described a high electron number density axially viewed ICP. Two ICP torch configurations were compared using 27- and 40-MHz RF generators and low aerosol carrier velocities. They employed conventional figures of analytical performance such as background, net line intensities, background equivalent concentrations (BECs), LODs, short- and long-term precision and freedom from EIE and solute vaporization interferences. The analytes investigated included both low energy and high-energy spectral wavelengths of Li, Na, K, P, Al, Fe, As, Zn, Pb, Ni, Mn, Cr, Cu, B, Co, Cd, Ti, V, Mo, Sn and Sr, and line pairs for Al, Pb, Fe and Mn. BECs and LODs differed by factors up to 3 among the test configurations. Houk and co-workers [8,29] generated a secondary discharge by extracting the axial channel of an ICP into a vacuum chamber via a water-cooled Cu sampler. The 27-MHz discharge was noticeably smaller and less intense than that produced from a 40-MHz plasma. Nakamura et al. [39,45] evaluated an axially viewed ICP using a high-resolution echelle spectrometer and compromise operating conditions owing to different spectral responses of the analyte lines.

4. Sample introduction

4.1. Liquids

Both conventional and unconventional modes of liquid sample introduction have been used with axially viewed ICPs. Fuxing et al. [17,18], used a specially designed high salt 'bell-mouth' pneumatic concentric nebulizer and a thermal desolvation system consisting of a heated spray chamber to determine trace elements in NaCl brines. No salt deposition occurred at the nebulizer orifice due to the optimum design of the bell-mouth extension.

A conventional glass concentric nebulizer was employed for the comparison of axially and radially viewed ICPs by Brenner et al. [36]. In that study, a glass cyclone spray chamber (Glass Expansion, Australia) was employed in the axial view study, while in the radial configuration, a Sturman-Masters vertical cyclonic spray chamber was used. The advantage of the glass cyclone spray chamber is the small void volume of approximately 50 ml, and as a result, rapid washout. Ivaldi and Tyson [34] and Brenner et al. [37] used a PE Ryton cross-flow Gem Tip nebulizer (CFN) and a PE Ryton spray chamber. Dahlquist et al. [46] used a Meinhard K (Santa Ana, CA) and an ARL (Ecublens, Switzerland) maximum dissolved solids V-groove nebulizer (MSDN) and observed that the precision varied from < 0.2 to 0.5%, respectively.

Ivaldi and Tyson [34] and Brenner et al. [36,37] determined the LODs and the influence of high Na and Ca concentrations in axially viewed ICPs using an USN and desolvation (Cetac Technologies, Omaha, NE). The desolvated aerosol was coupled directly to the base of the torch. The desolvation temperature was 140°C and the chiller was set at 0–2°C.

Dubuisson et al. [48] employed robust plasma conditions to minimize Na interference effects in the plasma and then to evaluate the role of the sample introduction system. They used a Perkin Elmer Conespray nebulizer with a cyclone spray chamber and a cross-flow nebulizer with a double pass spray chamber. The latter system was more sensitive to Na, finer droplets being obtained at the spray chamber exit when Na was present.

De Loos-Vollebregt et al. [4] used thermospray sample introduction and observed that LODs were enhanced fourfold relative to those obtained using a conventional pneumatic nebulizer. Conver et al. [51], used an axially viewed sequential ICP spectrometer (Varian Liberty) to evaluate the performance of a FSApT sample introduction system. These authors anticipated that the improved LODs would be further enhanced as a result of the increased sample transport. However, when FSApT was used with a standard axial torch having a large diameter (2.3 mm) injector, SBRs and background R.S.D.s were not improved in comparison to conventional pneumatic nebulization. With a smaller torch injector, %R.S.D.s for FSApT were similar to those obtained with a pneumatic sample introduction system, and larger LOD improvements were reported. It was con-

cluded that high-performance FSApt might be incompatible with axially viewed ICPs.

4.2. Gases

A direct injection probe (DIP) [26] was employed to analyze a gaseous mixture of Cl, Br, C and S compounds using a direct couple optical probe consisting of a He-purged water-cooled Cu-cone. The orifice of this cone, 3 mm in diameter, was immersed in the ICP. This interface facilitated the determination of elements using VUV spectral lines which otherwise would have been totally attenuated by absorption by atmospheric oxygen and by the optical components in the optical transfer system. Samples were introduced using flow injection (FIA).

5. Fundamental aspects

From a fundamental point of view, the axially viewed ICP does not differ from the radial configuration. There are, however, several points to be considered relative to the direction of viewing applied. In general, the ICP is sheathed by boundary layers that are substantially cooler (approx. 2400 K) than the plasma core and axial column (8000–1000 K). The energy in the hot plasma core rapidly diffuses outward by thermal conduction, electrons and ions migrating to the cooler peripheral region by ambipolar diffusion [73–75]. As a result of these processes, the ICP decays with increasing rapidity with increasing height above the load coil. If the electron number density (n_e), is the local thermal equilibrium (LTE) value as determined by the Saha equation, then at 20 mm above the load coil, the value will be considerably degraded relative to that of the NAZ. Montaser and Fassel [23] located a copper metal skimmer below the analytical observation zone to isolate the axial channel of the ICP and to deflect the outer cool fringe. The electron density was approximately 8.5×10^{13} cm^{-3} compared to 4×10^{14}–1.4×10^{15} cm^{-3} for a conventional ICP.

In the axially viewed ICP, the outer fringe of the ICP can strongly absorb the emission of atomic resonance lines [76]. Absorption profiles from these boundary regions indicate that the ratio of absorption to emitting populations is 10^9-fold larger than in the IRZ and NAZ. This fact should be taken into account in the determination of the plasma temperature by the ion-to-atom line intensity ratio method. Otherwise, the values can be significantly biased by boundary layer absorption if one of the spectral lines is a resonance line and the results will be skewed toward erroneously high Saha temperatures. Consequently, from the analytical aspect, when viewing the plasma in the axial end-on direction it is important that the cool plasma fringe be excluded.

6. Diagnostics — the Mg II 280.270 nm / Mg I 285.213 nm ratio

In many of the studies comparing EIEs, Ca and acid interference effects in axially and radially viewed ICPs, the Mg II 280.270 nm/Mg I 285.213 nm intensity ratio has been used as a practical criterion for plasma *robustness* and analytical performance. Mermet [43,49,50] coined the term *robustness* to collectively express energy transfer, residence time, and response of the plasma to changes in atomization and excitation conditions and chemical composition of the aspirated solution. The ratio is related to n_e by the Saha–Eggert equation, assuming LTE, and to ionization and excitation temperatures. Mermet [50] determined Mg II 280.270 nm/Mg I 285.213 nm intensity ratios in radially viewed plasmas produced in torches with different central injector diameters. He concluded that the Mg II/Mg I ratios approach LTE values at optimum energy transfer and residence times. Such conditions prevail when the internal diameter of the central torch injector exceeds 2 mm (gas velocity decreases), when the aerosol carrier flow rate is approximately 0.5–0.7 l min^{-1}, and the forward power is high [35–37,44,49,50,67–71]. With other less favorable conditions, the Mg II/Mg I ratios are significantly lower [34,37].

A compilation of available Mg II/Mg I data for various spectrometers, sample introduction sys-

tems (Meinhard concentric, CFN, modified Lichte, USN), and excitation systems is presented in Table 1 [34,36,37,40,41,44,77,79]. Original Optima 3000 XL intensity data were multiplied by 1.86 due to differences in echelle spectrometer sensitivity between the two Mg lines [34,80].

The data listed in Table 1 indicate that the ratios for axially viewed ICPs are lower than those obtained with radially viewed plasmas. The available data indicate that under similar conditions of aerosol flow rate (0.7–0.8 l min^{-1}), the ratios for the Varian Liberty, the TJA Solutions IRIS, Spectro and Jobin Yvon systems for *pure water* were higher than those observed for the Perkin Elmer Optima 3000 XL configuration. In the first group of instruments, ratios varied from approximately 10 at 1 kW to 13 at 1.5 kW, whereas in the latter system, the ratios varied from 7 at 1 kW to 9 at 1.35 kW.

Brenner et al. [36,37,44] measured the Mg II/Mg I ratio using a conventional concentric pneumatic nebulizer and a USN (Cetac Tech-

Table 1
Compilation of Mg II 280.270 nm/Mg I 285.213 nm ratios for various axially and radially viewed ICPs using conventional nebulization (Meinhard, cross-flow and modified Lichte) and USN, using various RF powers and sample composition[a]

Instrument	Solution	Liberty	Optima	IRIS	Liberty	Optima	Optima	Optima	EOP	EOP
Reference		36	34	79	36	37	34	40	77	89
Power (kW)		Radial	Radial	Radial	Axial	Axial	Axial	Axial	Axial	Axial
Conventional nebulization										
0.75	Water			6.5						
0.9–1	Water	10.5	5.2	9.5	10	7.1	5.9	8.5	6.2	
1.1–1.15	Water			10.3					7.9	
1.2–1.25	Water				11.4			9	9.1	9.5
1.3–1.35	Water			12.7		9.1			9.9	10.3
1.4–1.5	Water	12	7.3		11.9	9.7	5.9	10.5		11
0.9	10% acetic acid							9.8		
1.2	10% acetic acid							10.3		
1.5	10% acetic acid							12.2		
1	Na 0.1%	10.5			7	5.6				
1	Ca 0.1%	10.1			7	5.8				
1	NaCl 5%	6–7			6–7					
0.95	NaCl 10%		3.6				2			
1.35	Na 0.1%					7.4				
1.35	Ca 0.1%					7.6				
1.5	Na 0.1%					8				
1.5	Ca 0.1%					8.1				
USN										
1	Water					5.3				
1.2	Water					7.1				
1.35	Water	7.5			7	7.5				
1	Na 0.1%	7			5.5	2.7				
1	Ca 0.1%					2.2				
1.35–1.4	Na 0.1%	8			7	4.1				
K										
1.35	Na 0.1%									
1.35	Ca 0.1%					3.5				

[a] Original Optima 3000 XL data were multiplied by 1.86 as stated by Ivaldi and Tyson [34]. This is due to the different sensitivity of the two Mg lines in the PE echelle spectrometer.

nologies) in aqueous solutions at forward powers of 1 and 1.35 kW using 2- and 2.3-mm central torch injectors. Mg II/Mg I ratios increased with decreasing aerosol flow rate and increasing RF power [36]. In a desolvated plasma the Mg II/Mg I ratio was lower than that of an ICP containing water (approx. 11 vs. 7 in the Varian system and 7 and 5 in the Perkin Elmer Optima system). In desolvated plasmas, the excitation temperatures are lower than in a plasma containing water. Dissociation of moderate amount of water in the plasma results in the formation of hydrogen and as a result an increase of the excitation temperature in the central channel [7,70,81].

Ivaldi and Tyson [34] determined the Mg II/Mg I ratio in a pure aqueous solution and in 10% NaCl. For their radially and axially viewed ICPs, they reported significantly lower ratios of 5 and 6 for a RF power of 0.95 kW for an aqueous solution, which increased to 7.3 and 6 at 1.45 kW and an aerosol flow rate of 0.6 l min^{-1}, respectively. In the presence of 10% NaCl, the ratio was suppressed by up to a factor of 2. In comparison to the axial and radial configurations obtained with other systems, the setup employed by Ivaldi and Tyson [34] appears to have been less robust.

Brenner et al. [36,37] measured the Mg II/Mg I ratios for 0.1% Na and 0.1% Ca using conventional concentric (Meinhard) and CFN (Perkin Elmer) nebulizers and a USN (Cetac). Varian Liberty sequential and Perkin Elmer 3000 XL SCD spectrometers were used, employing 2.3- and 2-mm-diameter central torch injectors. Two RF power levels were applied — 1 and 1.35 kW. With the concentric and the CFN for 1 kW, ratios were approximately 7 for the Varian system [36] and approximately 6 for the Perkin Elmer [37]. In the presence of 0.1% Na the ratio was 5 for a CFN and only 2.7 for an USN at 1 kW. With the 0.1% Ca solution, the ratio was approximately 6 for the CFN and only 2 for the USN. These ratios increased when the RF power increased to 1.35 kW — 7.5 and 3.5, respectively. In general, these low ratios indicate that the plasma observation zone was less robust. In contrast, USN ratios using the Varian system were slightly higher — 5.5 at 1 kW and 7 at 1.35 kW. In the Spectro EOP, the Mg II/Mg I ratio was 9.5 using 1.2 kW and an aerosol flow rate of 0.9 l min^{-1}. At 1.4 kW, it was 11. Brenner et al. [44] measured the Mg II/Mg I intensity ratio for solutions containing 0.5% Ca and 0.5% Na. In the axially viewed ICP the ratio was 10.5 for pure water and for 0.5% Na. The ratio was 8 for 0.5% Ca. These values indicate that the ICP was robust even in the presence of high Na and Ca concentrations.

As mentioned previously, both radially and axially viewed Mg II/Mg I ratios vary with the diameter of the central injector of the torch. The values quoted by Ivaldi and Tyson [34] using a narrow-bore central torch injector were significantly lower than those listed by Brenner et al. [36,37,44], Dubuisson et al. [40] and Romero et al. [69] using similar instrumental and torch configurations but wider bore torch injectors (> 2 mm). Evidently, the diameter of the central torch injector has a large influence. According to Cooper [78], the Mg II/Mg I ratio increased from 6.5 at 0.75 kW to 12.7 at 1.35 kW for pure water. The ratios for the Spectro EOP system varied from approximately 6 at 1 kW to 10 at 1.3 kW (in both cases the diameter of the central injector was not stated).

Dubuisson et al. [40] used the Mg II/Mg I intensity ratio to compare axially and radially viewed ICPs with 10% acetic acid. Ratios increased with increasing power from approximately 10 and 8.5 at 0.9 kW to approximately 12 and 10.5 at 1.5 kW and an argon aerosol flow rate of 0.5 l min^{-1}. The ratio decreased to 2 at 1 l min^{-1} gas flow rate for acetic acid. The ratios for the acid were higher than those for pure water. They concluded that under robust plasma conditions, interferences in axial and radial configurations were of similar magnitude and that aerosol formation and transport processes were responsible for the observed variations. In the case of acetic acid, the increase of the Mg II/Mg I ratio was due to the relative increase in the Mg II signal attributed to the increase in ionization caused by an increase in temperature.

Todoli et al. [82] studied interference effects of HNO_3 and H_2SO_4 using several types of nebulizers; i.e. microconcentric (MCN) (Cetac), Meinhard concentric and Perkin Elmer Conespray, and attributed matrix effects to ionic distribution

phenomena, claiming that plasma effects were insignificant. However, the low Mg II/Mg I ratios of approximately 6.4–6.8 at 1.2 kW indicate that a non-robust plasma prevailed. Thus, RF power is an important parameter and an increase results in the reduction of matrix effects but at the expense of the LODs, which are degraded by factors of 2–6 due to the increase in background intensity.

7. Limits of detection and SBR

7.1. Conventional sample introduction

Nakamura et al. [39,45] determined the LODs in radially and axially viewed ICPs. A 5–35-fold net intensity enhancement in the axially viewed ICP was observed. In comparison to the radially viewed ICP, LODs were improved 1.4–25-fold and varied from 0.17 to 540 and 0.018 to 35 $\mu g\ l^{-1}$, respectively, for the radial and axial configurations, respectively. Dahlquist et al. [46], determined the LODs for Li, Na, K, P, Al, Fe, As, Zn, Pb, Ni, Mn, Cr, Cu, B, Co, Cd, Ti, V, Mo, Sn and Sr. Although the background for their axially viewed ICP was larger than that for radial viewing, net intensities were 6–13 times greater.

Montaser and Fassel [23] observed that SBRs and LODs of 10 atom lines having various excitation energies were 5–20 times superior to those obtained using a conventional configuration. The observation height (10–30 mm) did not have a great influence on the SBRs, which varied by up to a factor of 3.

Duffy and Thomas [83] determined B, P and S in low alloy steels using an Optima DV SCD spectrometer. The LODs for these elements were improved by factors of 5–10 in comparison to radially viewed ICPs. Recently, Dubuisson et al. [35] compared the SBRs of ion spectral lines of several commercially available axially and radially viewed ICP-AES systems. They observed that both analyte and background signals were higher for axial viewing, but SBRs were higher owing to the larger increase of signal relative to the background. They showed that up to threefold improvements could be obtained for axial viewing. However, these authors also noted a decrease in the dynamic range and an increase in interference effects. Nakamura et al. [39,45] determined the LODs of 24 elements using conventional and extended torches. LODs for the latter were improved by 50% for Be and up to sevenfold for Al.

A compilation of LODs obtained by axial and radial viewing using conventional nebulization and USN and various spectrometers is presented in Table 2. These data are reproduced from recent publications [34–37], manufacturer's brochures, information lists and written communications [64,77–79,84–91]. Ivaldi and Tyson [34] determined LODs using the Perkin Elmer Optima XL SCD spectrometer. Dubuisson et al. [35] and Brenner et al. [36,37] listed LODs (3σ) for a wide range of spectral lines varying in energy potentials, using Varian Liberty Series II [36] sequential and Perkin Elmer SCD multichannel [37] spectrometers using conventional pneumatic and USN.

Relative to radially viewed ICPs, mean detection limit improvement factors for axial configurations using conventional nebulization varied from approximately 2 to 20. LODs determined using the Perkin Elmer SCD system [37] were similar to the axially viewed values published by Brenner et al. [36] using a sequential ICP spectrometer (Varian, Liberty). In the presence of 5% NaCl, LODs were degraded approximately by a factor of 5 [36]. In the presence of 0.1% Na and 0.1% Ca, LODs were degraded by approximately one order of magnitude relative to those of an aqueous solution [37]. In general, LODs of Se, As and Tl were improved when the forward power increased from 1 to 1.35 kW.

It is of interest to note that radially viewed ICP LODs obtained with an optimized photon transmission sequential spectrometer with an optimized detection system (high S/N) (1 m Jobin Yvon Ultima) and a concentric nebulizer are within the range of axially viewed ICPs (Table 2). LODs, recently determined by Dubuisson et al. [91], using an axially viewed ICP and a similar sequential spectrometer (JY238) were improved by up to one order of magnitude (RF power 1 kW, carrier gas 0.75 l min^{-1}) and were mostly in the 10–100 ng l^{-1} range for the spectral lines

Table 2
Compilation of LODs (3σ, $\mu g\ l^{-1}$) for axially viewed ICPs in aqueous solution using conventional and ultrasonic nebulization[a]

Element	Wavelength	EP	IP	IP + EP	RP	RP	RP	RP	RP	RP	RP	AP	AP	AP	AP	AP
Reference	(nm)	(eV)	(eV)	(eV)	36	85,86	86	77,89	90	79	79	84,85	84,85	86	37	87
Sample introduction					Meinhard	Meinhard	Meinhard	Meinhard	Meinhard	Meinhard	USN	Meinhard	Meinhard	Meinhard	CFN	CFN
Instrument					Liberty	Liberty	Vista	Modula	61 E Trace	JY238	JY238	Liberty	Liberty	Vista	Optima	Optima
Manufacturer					Varian	Varian	Varian	Spectro	TJA	JY	JY	Varian	Varian	Varian	PE	PE
Ag I	328.068	3.78	7.58	11.36	5	2	2	1.9	0.5	0.6	0.08		0.7	0.5		0.4
Al II	167.081	7.42	5.99	13.41			1	0.35						0.5		
Al I	308.215	4.02	5.99	10.01				10		4.7						4
Al I	396.152	3.14	5.99	9.13		3	6			0.2	0.02	1	0.7	1.5		2
As I	189.042	6.56	9.81	16.37	12	9	22	11	2	0.8	0.2	10	6	5	8.2	2
As I	193.759	6.4	9.81	16.21	10		20	2				4		5	6.1	5
As I	197.197	6.29	9.81	16.1			63							16	23	
Au I	242.795	5.1	9.23	14.33		4	7	3.7	0.6	0.6			0.4	1.4		
Au I	267.595	4.63	9.23	13.86		4	9							1.4		
B I	182.64	6.79	8.3	15.09		4.5	1	2.7		0.3	0.03		4	0.3		
B I	208.959	5.94	8.3	14.24			2.1							0.7		
B I	249.773	4.96	8.3	13.26		1	0.3	1.4	0.8				0.4	0.07		0.5
Ba II	233.527	6	5.21	11.21			1.1							0.2		
Ba II	455.403	2.72	5.21	7.93	0.1	0.06	0.3	0.2		0.05	0.004	0.01	0.01	0.04		0.07
Ba II	493.409	2.51	5.21	7.72			0.3		0.06					0.05		
Be I	234.861	5.28	9.32	14.6	0.15	0.15	0.3	0.06	0.06	0.05	0.004	0.05	0.05	0.05	0.09	
Be II	313.042	3.96	9.32	13.28			0.05	0.06						0.3	0.17	0.08
Be II	313.107	3.96	9.32	13.28											0.12	
Bi I	223.061	5.55	7.29	12.84		9	18	15	2	2.6			0.8	3		2
Br I	157.484	8.33	11.81	20.14				580								
Br I	163.34	8.05	11.81	19.86												
Ca I	317.933	7.04	6.11	13.15			4	2.5					1.7	1		2
Ca II	393.366	3.15	6.11	9.26		0.03	0.08	0.07		0.03	0.003		0.005	0.01		
Ca II	396.847	3.12	6.11	9.23			0.07		0.03					0.01		
Cd II	214.438	5.78	8.99	14.77			1.5			0.06	0.02			0.3	0.97	0.3
Cd II	226.502	5.47	8.99	14.46	2		1.2	0.59		0.09		0.15		0.3	1	0.2
Cd I	228.802	5.41	8.99	14.4		1.2		0.85	0.09				0.3		0.92	0.3
Ce II	413.765	3.52	5.47	8.99		6	26							2.2		
Ce II	418.66	3.82	5.47	9.29			11							2		
Cl I	134.724	9.2	12.97	22.17				50								
Cl I	857.527	10.47	12.97	23.44		20 000							5000			
Co II	228.616	5.84	7.86	13.7		4	3.5	2.2	0.5				0.3	0.8	1.3	0.5
Co II	230.786	5.87	7.86	13.73											2.5	
Co II	237.862	5.62	7.86	13.48			4.5							0.7		
Co II	238.892	5.6	7.86	13.46	4		4.5			0.21	0.04	0.25		0.5	0.95	0.4
Cr II	205.552	6.03	6.77	12.8			4	1.5						0.7	1.1	0.4
Cr II	206.149	6.02	7.77	13.79										1.4	1.2	0.6
Cr II	267.716	6.18	6.77	12.95	4	3	2	1.5	0.4	0.15	0.04	0.2	0.3	0.5	0.3	0.2
Cu II	224.7	8.23	7.73	15.96											0.4	
Cu I	324.754	3.82	7.73	11.55	2	1.5	1.8	1.1	0.3	0.1	0.03	0.6	0.5	0.3		0.5
Cu I	327.396	3.78	7.73	11.51			2							0.6	1.8	0.2
Dy II	340.779	3.63	5.93	9.56			5							0.6		
Dy II	353.17	3.5	5.93	9.43			2							0.3		
Dy II	364.541	3.5	5.93	9.43			4							0.5		

Table 2 (*Continued*)

Element	Wavelength	EP	IP	IP + EP	RP	RP	RP	RP	RP	RP	RP	AP	AP	AP	AP	AP
Reference	(nm)	(eV)	(eV)	(eV)	36	85,86	86	77,89	90	79	79	84,85	84,85	86	37	87
Sample introduction					Meinhard	Meinhard	Meinhard	Meinhard	Meinhard	Meinhard	USN	Meinhard	Meinhard	Meinhard	CFN	CFN
Instrument					Liberty	Liberty	Vista	Modula	61 E Trace	JY238	JY238	Liberty	Liberty	Vista	Optima	Optima
Manufacturer					Varian	Varian	Varian	Spectro	TJA	JY	JY	Varian	Varian	Varian	PE	PE
Er II	337.276	3.67	6.1	9.77			2.1							0.2		
Er II	349.91	3.59	6.1	9.69			2.2							0.4		
Eu II	412.973	3	5.67	8.67			1.3							0.1		
Eu II	420.505	2.95	5.67	8.62			0.8							0.06		
Fe II	238.204	5.2	7.87	13.07			2.3							0.35		0.5
Fe II	239.562	5.2	7.87	13.07											2.2	
Fe II	259.94	5.22	7.87	13.09	1.5	0.3	5	1.1	0.3	0.2	0.05	0.3	0.2	0.4		0.3
Fe II	273.955	5.51	7.87	13.38											1.6	
Ga I	287.424	4.31	6	10.31			38							3.2		
Ga I	294.364	4.31	6	10.31			20							2		
Ga I	417.206	3.07	6	9.07			50							2.6		
Gd II	335.047	3.85	6.14	9.99			4							0.5		
Gd II	336.223	3.77	6.14	9.91			5							0.6		
Gd II	342.247	3.86	6.14	10		2.5	3							0.5		
Ge I	206.866	6.06	7.88	13.94			30							5.4		
Ge I	265.118	4.85	7.9	12.75			26	7.8						4		
Hf II	277.336	5.25	6.6	11.85			7							1		
Hg I	184.95	6.67	10.44	17.11			9	6.5		1.2	0.3		2	2		
Hg II	194.227	6.39	10.44	16.83		7	11							2		0.5
Hg I	253.652	4.88	10.44	15.32			18							3		
Ho II	339.898	3.65	6.02	9.67			3.6							0.5		
Ho II	345.6	3.65	8.78	12.43		0.45	2.5							0.2		
I I	142.549	8.7	10.45	19.15												
I I	161.76	7.66	10.45	18.11				270								
I I	178.215	6.95	10.45	17.4			6							0.9		
I I	179.847	7.83	10.45	18.28			31							9		
In II	230.606	5.37	5.79	11.16			32	31						4		
In I	325.609	4.08	5.79	9.87		14										
Ir II	212.681	5.83	9	14.83			11							2		
Ir II	224.268	5.53	9	14.53			17							2.1		
K I	766.49	1.62	4.34	5.96	10		6.5	27	15	6	0.9	3	8	0.5		2
K I	769.896	1.61	4.34	5.95			43							1.3		
La II	333.749	4.12	4.34	8.46			2.2							0.35		
La II	379.478	3.51	5.58	9.09		0.015	2							0.3		
La II	408.672	3.03	5.58	8.61			1.7							0.35		
Li I	610.364	3.87	5.39	9.26			27							1.3	1.9	
Li I	670.784	1.85	5.39	7.24	1	0.5	0.4	0.9		0.4	0.05	0.12	0.05	0.1	0.1	
Lu II	261.139	4.74	5.42	10.16			0.3							0.05		
Mg II	279.079	8.86	7.65	16.51				11							2.5	0.05
Mg II	279.553	4.43	7.65	12.08		0.08	0.09	0.05	0.03	0.03	0.003		0.02	0.01		
Mg II	280.27	4.42	7.65	12.07			0.3							0.04	0.12	
Mg I	285.213	4.34	7.65	11.99			2.7							0.08		

Table 2 (*Continued*)

Element	Wavelength	EP	IP	IP + EP	RP	RP	RP	RP	RP	RP	RP	AP	AP	AP	AP	AP
Reference	(nm)	(eV)	(eV)	(eV)	36	85,86	86	77,89	90	79	79	84,85	84,85	86	37	87
Sample introduction					Meinhard	Meinhard	Meinhard	Meinhard	Meinhard	Meinhard	USN	Meinhard	Meinhard	Meinhard	CFN	CFN
Instrument					Liberty	Liberty	Vista	Modula	61 E Trace	JY238	JY238	Liberty	Liberty	Vista	Optima	Optima
Manufacturer					Varian	Varian	Varian	Spectro	TJA	JY	JY	Varian	Varian	Varian	PE	PE
Mn II	257.61	4.81	7.44	12.25	0.2	0.3	0.3	0.17		0.05	0.009	0.06	0.02	0.05	0.07	0.1
Mn II	259.373	4.77	7.44	12.21			0.6							0.08		
Mn II	260.569	4.75	7.44	12.19			1.8		0.05					0.2	0.14	
Mo II	202.03	6.13	7.1	13.23	4	3	5	2.2	0.5	0.2	0.05	0.6	0.6	0.8	1.7	0.7
Mo II	203.844	6.08	7.1	13.18											4.1	
Mo II	204.598	6.06	7.1	13.16											5.1	
N I	174.525	10.67	14.53	25.2												
Na I	588.995	2.1	5.14	7.24		0.8	2		0.9				0.3	0.1		
Na I	589.592	2.1	5.14	7.24			1	8.2		0.3	0.06			0.2		3
Nb II	309.418	4.52	6.88	11.4			14							0.7		
Nb II	313.078	4.4	6.88	11.28			7							0.7		
Nd II	401.225	3.71	5.49	9.2			8							0.7		
Nd II	406.109	3.52	5.49	9.01			10							0.7		
Ni II	221.647	6.03	7.64	13.67	5		10							1.5	1.9	0.9
Ni II	231.604	6.39	7.64	14.03		5	10	2.5	0.5			0.75	0.6	1.3	1.7	0.7
Ni II	232.003	5.34	7.64	12.98											3.2	
Os I	225.585	5.49	8.73	14.22			7							0.9		
P I	177.499	6.99	10.49	17.48		15	17						8	7		
P I	178.287	6.95	10.49	17.44		25	19	8.5					9	9		
P I	213.618	7.22	10.49	17.71		13.5	16						10			
Pb II	168.215	7.37	7.42	14.79	12			31		1.5	0.4					
Pb I	216.999	5.71	7.42	13.13											11	
Pb II	220.353	7.37	7.42	14.79		11	17	14	0.8	1.5		1.5	2	3	2	0.8
Pd I	340.458	4.46	8.34	12.8			12	3.8						1.5		
Pd I	360.955	4.4	8.34	12.74			28							3		
Pr II	390.844	3.17	5.42	8.59			10							0.9		
Pr II	417.939	3.17	5.42	8.59			9							1.3		
Pt II	214.423	5.8	9	14.8			19							3		
Pt I	265.945	4.66	9	13.66			38	18						4		
Rb I	780.023	1.59	4.18	5.77			5							1		
Re II	197.228	6.3	7.87	14.17			9.5							0.9		
Re II	227.525	5.44	7.87	13.31			10							0.9		
Rh II	249.077	7.07	7.45	14.52			22							3.8		
Rh II	343.489	3.6	7.45	11.05			19							2		
Ru II	240.273	6.29	7.37	13.66			11							1.1		
Ru II	245.644	6.39	7.37	13.76				14								
Ru II	267.876	5.76	7.37	13.13			8							0.6		
S I	180.734	6.85	10.36	17.21		15	36						5	13		
S I	182.036	6.85	10.36	17.21		36	35	13					10	9		
Sb I	206.833	5.98	8.64	14.62			28		2	1.5				2.9	8	2
Sb I	217.581	5.69	8.64	14.33		14		8.4		1.5	0.3		2.5		5	2
Sb I	231.147	5.36	8.64	14			36							2		
Sc II	255.238	4.88	6.54	11.42												
Sc II	361.384	3.45	6.54	9.99		0.3	0.5	0.22	0.05	0.09				0.06		

Table 2 (*Continued*)

Element	Wavelength	EP	IP	IP + EP	RP	RP	RP	RP	RP	RP	RP	AP	AP	AP	AP	AP
Reference	(nm)	(eV)	(eV)	(eV)	36	85,86	86	77,89	90	79	79	84,85	84,85	86	37	87
Sample introduction					Meinhard	Meinhard	Meinhard	Meinhard	Meinhard	Meinhard	USN	Meinhard	Meinhard	Meinhard	CFN	CFN
Instrument					Liberty	Liberty	Vista	Modula	61 E Trace	JY238	JY238	Liberty	Liberty	Vista	Optima	Optima
Manufacturer					Varian	Varian	Varian	Spectro	TJA	JY	JY	Varian	Varian	Varian	PE	PE
Se I	196.026	6.32	9.75	16.07	30	30	33	15	2	1.5	0.4	3	4	5	7.4	2
Se I	203.985	6.32	9.75	16.07			65							15	31	
Si I	212.412	6.62	8.15	14.77			12							2.8		
Si I	251.611	4.95	8.15	13.1		4	12	3.1		1.5	0.2		0.5	1.7		
Si I	288.158	5.08	8.15	13.23			8		2					1.5		
Sm II	359.262	3.83	5.6	9.43			4.5							0.7		
Sm II	360.979	3.71	5.6	9.31			7							0.7		
Sn II	189.989	7.05	7.34	14.39		23	27	10		1.3			3.5	3		
Sr II	407.771	3.04	5.7	8.74	0.03	0.015	0.07	0.07		0.03	0.005	0.01	0.004	0.005	0.04	
Sr II	421.552	2.94	5.7	8.64			0.1		0.03					0.01	0.01	0.1
Ta II	240.063	5.93	7.89	13.82			47	5.6						1.3		
Ta II	268.516	4.6	7.89	12.49			48							1.5		
Tb II	350.917	3.53	5.85	9.38			4							0.7		
Tb II	367.635	3.5	5.85	9.35			7.5							1.4		
Te I	214.275	5.78	9.01	14.79			35	19						6		
Th II	274.716	4.51	6.95	11.46		14										
Th II	283.73	5.14	6.95	12.09			10							1.3		
Ti II	334.941	3.74	6.82	10.56	0.6	0.5	0.5	0.45	0.09	0.03		0.07	0.05	0.13	0.2	0.7
Ti II	336.121	3.71	6.82	10.53			1.1	0.43						0.2	6.5	
Ti II	337.279	3.68	6.82	10.5			2							0.3		0.2
Ti II	345.666	5.09	6.82	11.91											8.6	
Tl II	190.8	6.49	6.11	12.6		12	24	19	2	1	0.3		3	5	25	2
Tl	276.787	4.48	6.11	10.59											1.7	
Tm II	313.126	3.96	6.18	10.14			1.3							0.3		
U I	385.958	3.24	6.08	9.32		14	18	9.4						5		
V II	270.094	4.63	6.74	11.37											1.8	
V II	292.402	4.63	6.74	11.37	2		3.5	2.6	0.5	0.19	0.05	0.8		0.4	0.25	0.4
V II	309.311	4.4	6.74	11.14		1.5	4.5						0.6	0.3		
V II	310.23	6.02	6.74	12.76											11.1	
V II	311.071	4.33	6.74	11.07				1.5								
W II	207.911	6.72	7.98	14.7		14	17	8.6						3		
W II	239.709	5.56	7.98	13.54												
W II	248.923	5.56	7.98	13.54			23							3.5		
Y II	371.029	3.52	6.38	9.9		0.15	0.7		0.3	1				0.1		
Yb II	328.93	3.77	6.25	10.02			0.2							0.03		
Yb II	369.419	3.35	6.25	9.6			0.4							0.05		
Zn II	202.548	6.12	9.39	15.51		0.8	1.1						0.2	0.80	0.97	0.3
Zn II	206.191	6.01	9.39	15.4			5	0.5						1.5	2.2	
Zn II	213.856	5.8	9.39	15.19	1		1		0.06	0.07	0.02	0.4	0.3	0.87	0.1	
Zr II	339.198	3.82	6.84	10.66		1.2	2.2		0.6					0.3		
Zr II	343.823	3.69	6.84	10.53		1.5	2	0.71		0.3			0.2	0.3		
Zr II	349.621	3.58	6.84	10.42			2.4							0.5		
Mean LOD					5.08	6.53	11.03	21.42	1.13	0.84	0.13	1.28	1.56	1.79	3.20	1.00

Table 2 (*Continued*)

Element	Wavelength	EP	IP	IP + EP	AP	AP	AP	AP	AP	AP	AP	AP	AP	AP	AP
Reference	(nm)	(eV)	(eV)	(eV)	34	35	87	88	91	77,89	77,89	37	36	84,85	91
Sample introduction					CFN	CFN	CFN	Meinhard	GEx	Meinhard	USN	USN	USN	USN	USN
Instrument					Optima	Optima	Optima	Panorama	JY138	EOP	EOP	Optima	Liberty	Liberty	JY138
Manufacturer					PE	PE	PE	JY	JY	Spectro	Spectro	PE	Varian	Varian	JY
Ag I	328.068	3.78	7.58	11.36			0.2	0.3		0.53				0.06	
Al II	167.081	7.42	5.99	13.41						0.15					
Al I	308.215	4.02	5.99	10.01						10					
Al I	396.152	3.14	5.99	9.13	0.5		7	1		0.2			0.15	0.15	
As I	189.042	6.56	9.81	16.37	5			3.9		6.8		2.2		0.6	
As I	193.759	6.4	9.81	16.21	5					7.8		1.5	1		
As I	197.197	6.29	9.81	16.1								3.2			
Au I	242.795	5.1	9.23	14.33						0.75					
Au I	267.595	4.63	9.23	13.86											
B I	182.64	6.79	8.3	15.09				0.7		7					
B I	208.959	5.94	8.3	14.24											
B I	249.773	4.96	8.3	13.26			0.2			0.39					
Ba II	233.527	6	5.21	11.21											
Ba II	455.403	2.72	5.21	7.93	0.04		0.2	0.24		0.1			0.005	0.003	
Ba II	493.409	2.51	5.21	7.72											
Be I	234.861	5.28	9.32	14.6	0.01	0.08		0.43		0.02	0.015	0.002	0.005	0.003	
Be II	313.042	3.96	9.32	13.28			0.07			0.02		0.01			
Be II	313.107	3.96	9.32	13.28								0.009			
Bi I	223.061	5.55	7.29	12.84						2.8					
Br I	157.484	8.33	11.81	20.14						300					
Br I	163.34	8.05	11.81	19.86						250					
Ca I	317.933	7.04	6.11	13.15			7			0.35					
Ca II	393.366	3.15	6.11	9.26				0.05		0.068					
Ca II	396.847	3.12	6.11	9.23											
Cd II	214.438	5.78	8.99	14.77			0.2					0.12			
Cd II	226.502	5.47	8.99	14.46	0.3	0.2		0.2	0.045	0.19	0.075	0.1	0.05		0.008
Cd I	228.802	5.41	8.99	14.4						0.22		0.04		0.04	
Ce II	413.765	3.52	5.47	8.99											
Ce II	418.66	3.82	5.47	9.29											
Cl I	134.724	9.2	12.97	22.17						50					
Cl I	857.527	10.47	12.97	23.44											
Co II	228.616	5.84	7.86	13.7						0.35		0.067		0.03	
Co II	230.786	5.87	7.86	13.73								0.18			
Co II	237.862	5.62	7.86	13.48											
Co II	238.892	5.6	7.86	13.46	0.2	0.4		0.5	0.11	0.5		0.06	0.05		0.01
Cr II	205.552	6.03	6.77	12.8					0.065	0.1		0.12			0.01
Cr II	206.149	6.02	7.77	13.79							0.06				
Cr II	267.716	6.18	6.77	12.95	0.2	0.2	1.1	0.5		0.35	0.1	0.03	0.03	0.03	
Cu II	224.7	8.23	7.73	15.96								0.14			
Cu I	324.754	3.82	7.73	11.55	0.25	0.5	1.5	0.5		0.82			0.05	0.03	
Cu I	327.396	3.78	7.73	11.51								0.08			
Dy II	340.779	3.63	5.93	9.56											
Dy II	353.17	3.5	5.93	9.43											
Dy II	364.541	3.5	5.93	9.43											

Table 2 (*Continued*)

Element	Wavelength	EP	IP	IP + EP	AP	AP	AP	AP	AP	AP	AP	AP	AP	AP	AP
Reference	(nm)	(eV)	(eV)	(eV)	34	35	87	88	91	77,89	77,89	37	36	84,85	91
Sample introduction					CFN	CFN	CFN	Meinhard	GEx	Meinhard	USN	USN	USN	USN	USN
Instrument					Optima	Optima	Optima	Panorama	JY138	EOP	EOP	Optima	Liberty	Liberty	JY138
Manufacturer					PE	PE	PE	JY	JY	Spectro	Spectro	PE	Varian	Varian	JY
Er II	337.276	3.67	6.1	9.77											
Er II	349.91	3.59	6.1	9.69											
Eu II	412.973	3	5.67	8.67											
Eu II	420.505	2.95	5.67	8.62											
Fe II	238.204	5.2	7.87	13.07					0.11						0.01
Fe II	239.562	5.2	7.87	13.07								0.09			
Fe II	259.94	5.22	7.87	13.09	0.15	0.3	0.7	0.4		0.3			0.04	0.03	
Fe II	273.955	5.51	7.87	13.38					0.70						
Ga I	287.424	4.31	6	10.31											
Ga I	294.364	4.31	6	10.31											
Ga I	417.206	3.07	6	9.07											
Gd II	335.047	3.85	6.14	9.99											
Gd II	336.223	3.77	6.14	9.91											
Gd II	342.247	3.86	6.14	10											
Ge I	206.866	6.06	7.88	13.94											
Ge I	265.118	4.85	7.9	12.75						16					
Hf II	277.336	5.25	6.6	11.85											
Hg I	184.95	6.67	10.44	17.11				2		3.3					
Hg II	194.227	6.39	10.44	16.83											
Hg I	253.652	4.88	10.44	15.32											
Ho II	339.898	3.65	6.02	9.67											
Ho II	345.6	3.65	8.78	12.43											
I I	142.549	8.7	10.45	19.15						10					
I I	161.76	7.66	10.45	18.11						53					
I I	178.215	6.95	10.45	17.4											
I I	179.847	7.83	10.45	18.28											
In II	230.606	5.37	5.79	11.16						5.3					
In I	325.609	4.08	5.79	9.87											
Ir II	212.681	5.83	9	14.83											
Ir II	224.268	5.53	9	14.53											
K I	766.49	1.62	4.34	5.96	3			1		2.2			0.6	1	
K I	769.896	1.61	4.34	5.95											
La II	333.749	4.12	4.34	8.46											
La II	379.478	3.51	5.58	9.09											
La II	408.672	3.03	5.58	8.61											
Li I	610.364	3.87	5.39	9.26								0.08			
Li I	670.784	1.85	5.39	7.24	0.2			0.2		0.11		0.02	0.06		
Lu II	261.139	4.74	5.42	10.16											
Mg II	279.079	8.86	7.65	16.51			1			2.7		0.13			
Mg II	279.553	4.43	7.65	12.08				0.04		0.03					
Mg II	280.27	4.42	7.65	12.07								0.01			
Mg I	285.213	4.34	7.65	11.99											
Mn II	257.61	4.81	7.44	12.25	0.03		0.9	0.1	0.017	0.04		0.01	0.005	0.003	0.002
Mn II	259.373	4.77	7.44	12.21											
Mn II	260.569	4.75	7.44	12.19								0.02			

Table 2 (*Continued*)

Element	Wavelength	EP	IP	IP + EP	AP	AP	AP	AP	AP	AP	AP	AP	AP	AP	AP
Reference	(nm)	(eV)	(eV)	(eV)	34	35	87	88	91	77,89	77,89	37	36	84,85	91
Sample introduction					CFN	CFN	CFN	Meinhard	GEx	Meinhard	USN	USN	USN	USN	USN
Instrument					Optima	Optima	Optima	Panorama	JY138	EOP	EOP	Optima	Liberty	Liberty	JY138
Manufacturer					PE	PE	PE	JY	JY	Spectro	Spectro	PE	Varian	Varian	JY
Mo II	202.03	6.13	7.1	13.23	0.2	0.7		0.45		0.6		0.06	0.04		
Mo II	203.844	6.08	7.1	13.18								0.19			
Mo II	204.598	6.06	7.1	13.16								0.35			
N I	174.525	10.67	14.53	25.2						100 mg l^{-1}					
Na I	588.995	2.1	5.14	7.24										0.03	
Na I	589.592	2.1	5.14	7.24				1.5		1.6					
Nb II	309.418	4.52	6.88	11.4											
Nb II	313.078	4.4	6.88	11.28											
Nd II	401.225	3.71	5.49	9.2											
Nd II	406.109	3.52	5.49	9.01											
Ni II	221.647	6.03	7.64	13.67								0.11			
Ni II	231.604	6.39	7.64	14.03	0.50	0.7	0.3	1	0.19	0.6	0.18	0.02	0.06	0.06	
Ni II	232.003	5.34	7.64	12.98								0.16			
Os I	225.585	5.49	8.73	14.22											
P I	177.499	6.99	10.49	17.48											
P I	178.287	6.95	10.49	17.44						4					
P I	213.618	7.22	10.49	17.71					1.1						0.13
Pb II	168.215	7.37	7.42	14.79						4.5					
Pb I	216.999	5.71	7.42	13.13								0.36			
Pb II	220.353	7.37	7.42	14.79	1.5	0.8	0.8	2.8	0.68	2.6	0.6	0.55	0.2	0.2	0.06
Pd I	340.458	4.46	8.34	12.8						3.1					
Pd I	360.955	4.4	8.34	12.74											
Pr II	390.844	3.17	5.42	8.59											
Pr II	417.939	3.17	5.42	8.59											
Pt II	214.423	5.8	9	14.8											
Pt I	265.945	4.66	9	13.66						4.9					
Rb I	780.023	1.59	4.18	5.77											
Re II	197.228	6.3	7.87	14.17											
Re II	227.525	5.44	7.87	13.31											
Rh II	249.077	7.07	7.45	14.52											
Rh II	343.489	3.6	7.45	11.05											
Ru II	240.273	6.29	7.37	13.66											
Ru II	245.644	6.39	7.37	13.76						18					
Ru II	267.876	5.76	7.37	13.13											
S I	180.734	6.85	10.36	17.21											
S I	182.036	6.85	10.36	17.21			1.4		6.6						
Sb I	206.833	5.98	8.64	14.62			1					0.93			
Sb I	217.581	5.69	8.64	14.33				2.7		2		0.63		0.2	
Sb I	231.147	5.36	8.64	14											
Sc II	255.238	4.88	6.54	11.42											
Sc II	361.384	3.45	6.54	9.99				0.08		0.24					
Se I	196.026	6.32	9.75	16.07	4		1.6	4.9		5.6		0.59	0.8	0.8	
Se I	203.985	6.32	9.75	16.07								1.7			

Table 2 (*Continued*)

Element	Wavelength	EP	IP	IP + EP	AP	AP	AP	AP	AP	AP	AP	AP	AP	AP	AP
Reference	(nm)	(eV)	(eV)	(eV)	34	35	87	88	91	77,89	77,89	37	36	84,85	91
Sample introduction					CFN	CFN	CFN	Meinhard	GEx	Meinhard	USN	USN	USN	USN	USN
Instrument					Optima	Optima	Optima	Panorama	JY138	EOP	EOP	Optima	Liberty	Liberty	JY138
Manufacturer					PE	PE	PE	JY	JY	Spectro	Spectro	PE	Varian	Varian	JY
Si I	212.412	6.62	8.15	14.77											
Si I	251.611	4.95	8.15	13.1						1.2					
Si I	288.158	5.08	8.15	13.23											
Sm II	359.262	3.83	5.6	9.43											
Sm II	360.979	3.71	5.6	9.31											
Sn II	189.989	7.05	7.34	14.39				1.4		2.2					
Sr II	407.771	3.04	5.7	8.74	0.01			0.007		0.05		0.02	0.005		
Sr II	421.552	2.94	5.7	8.64								0.02			
Ta II	240.063	5.93	7.89	13.82						1.3					
Ta II	268.516	4.6	7.89	12.49											
Tb II	350.917	3.53	5.85	9.38											
Tb II	367.635	3.5	5.85	9.35											
Te I	214.275	5.78	9.01	14.79						3.5					
Th II	274.716	4.51	6.95	11.46											
Th II	283.73	5.14	6.95	12.09											
Ti II	334.941	3.74	6.82	10.56	0.1	0.7		0.18		0.37		0.01	0.03		
Ti II	336.121	3.71	6.82	10.53						0.14		0.02			
Ti II	337.279	3.68	6.82	10.5											
Ti II	345.666	5.09	6.82	11.91								0.44			
Tl II	190.8	6.49	6.11	12.6			0.8	3.3		3.5	0.45	2.2		0.5	
Tl	276.787	4.48	6.11	10.59								1.34			
Tm II	313.126	3.96	6.18	10.14											
U I	385.958	3.24	6.08	9.32						23					
V II	270.094	4.63	6.74	11.37								0.25			
V II	292.402	4.63	6.74	11.37	0.3	0.4		0.4		0.51		0.01	0.05		
V II	309.311	4.4	6.74	11.14										0.05	
V II	310.23	6.02	6.74	12.76								9.4			
V II	311.071	4.33	6.74	11.07						0.22					
W II	207.911	6.72	7.98	14.7						2.6					
W II	239.709	5.56	7.98	13.54											
W II	248.923	5.56	7.98	13.54											
Y II	371.029	3.52	6.38	9.9				0.02							
Yb II	328.93	3.77	6.25	10.02											
Yb II	369.419	3.35	6.25	9.6											
Zn II	202.548	6.12	9.39	15.51								0.3		0.06	
Zn II	206.191	6.01	9.39	15.4						0.3		0.35			
Zn II	213.856	5.8	9.39	15.19	0.06	0.1	0.8	0.4	0.04			0.06	0.1		0.005
Zr II	339.198	3.82	6.84	10.66											
Zr II	343.823	3.69	6.84	10.53				0.07		0.73					
Zr II	349.621	3.58	6.84	10.42											
Mean LOD					1.03	0.42	1.30	0.99	0.24	12.71	0.24	0.58	0.23	0.19	0.03

[a]*Notes.* Spectro, USN no spectral lines quoted. JY 138 Ultratrace data, no spectral lines quoted. Axial data are for JY Panoramo polychromator, information sheet, January 1996. TJA ICAP 61 E Trace Analyzer information sheet. Varian Liberty Series II LOD information sheet, 1997. Data for RP, AP and USN.

selected. In the presence of 1% NaCl, these LODs were only degraded by a factor of 2. This is in marked contrast to data obtained by Brenner et al. using a CFN, where in the presence of 0.1% NaCl, LODs were degraded on the average by an order of magnitude [37]. With a microconcentric nebulizer (MCN 6000, Cetac Technologies), and an axially viewed ICP, Dubuisson et al. [91] cited LODs that were degraded only by a factor of approximately 5.

7.2. Enhanced sample introduction

Table 2 also lists USN LODs quoted in vendor brochures and obtained by Ivaldi and Tyson [34], Brenner et al. [36,37] and Dubuisson et al. [91] (a 1-m JY 238 sequential spectrometer was employed). In Brenner et al. [36], a Varian Series II sequential spectrometer was used and in Ivaldi and Tyson [34] and Brenner et al. [37], a Perkin Elmer Optima XL 3000 SCD system was employed.

In an aqueous solution, LODs can be further improved by more than one order of magnitude when an USN and desolvation is employed; i.e. a mean factor of approximately 50 over that obtained with conventional radial observation. Dubuisson et al. [91] cited USN LODs in the 2–100-ng l^{-1} range. It should be noted that the extent of enhancement is not uniform, and broadly depended on energy potentials of spectral lines, ICP operating conditions and composition of aspirated solutions.

Brenner et al. [37], determined the LODs in 0.1% Ca and Na using a USN. These were degraded by a factor of 30. However, relative to a CFN, USN LODs in 0.1% Na and Ca were still enhanced by a factor of 10. It was concluded that improvement of axial view LODs using USN extends the scope for trace element determinations in environmental, geochemical, biological samples.

LODs for concentrated acetic acid using radially and axially viewed ICPs (Modula and EOP), respectively, were significantly degraded by up to one order of magnitude [77] (Table 2, Fig. 5). The magnitude of degradation was not the same for all elements. Fig. 5 indicates that there is a broad

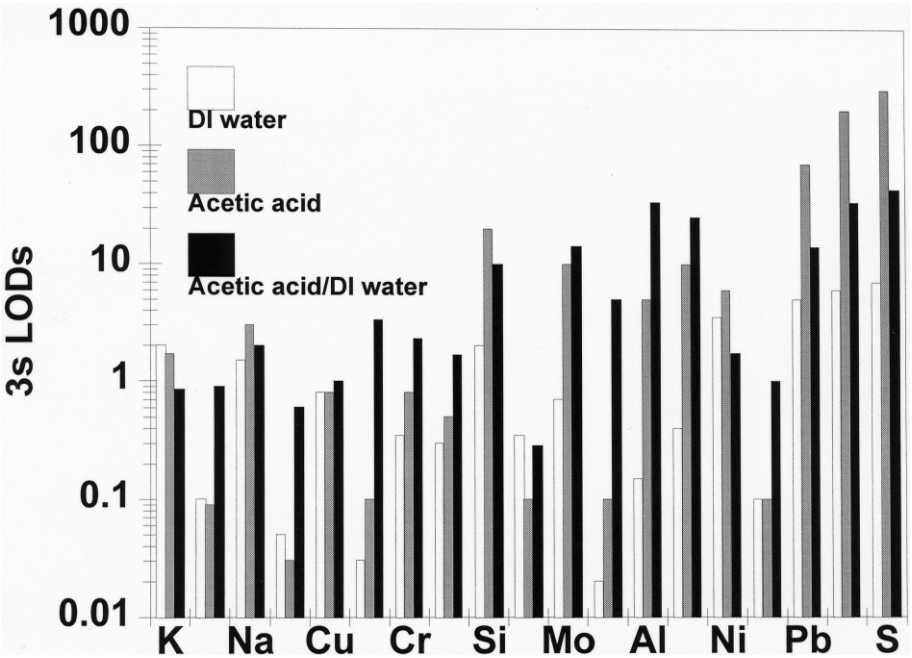

Fig. 5. Limits of detection ($\mu g\ l^{-1}$) in concentrated acetic acid using axially viewed ICPs. Data from Greb and Leitken [77], are arranged in increasing energy potential sum of the spectral lines and the element.

relation between degradation and energy potential of the spectral lines used (plotted in order of increasing energy potential of the spectral line and the element).

De Loos-Vollebregt et al. [4] used a thermospray with an axially viewed low-flow water-cooled ICP. LODs were improved by a factor of 4, but were degraded in comparison to state of art LODs listed in Table 2. Conver et al. [51], evaluated a fused silica-aperture thermospray nebulizer (FSApT). LODs were enhanced by a factor of 10 in comparison to pneumatic sample introduction. In comparison to FSApT with radial viewing, axially viewed LODs were only improved by a factor of 2. This small improvement suggested that axially viewed ICPs might not benefit from this mode of sample introduction. Nevertheless, improvement factors for FSApT with axially viewed ICPs are approximately 70 times those obtained with radially viewed plasmas with pneumatic nebulization (see Table IV in [51]).

Axially viewed LODs for water immiscible organic solvents are sparse. Fig. 6 compares axially viewed LODs in kerosene [77] with values obtained using a radially viewed ICP. Aqueous values from Table 2 are included for comparison. Axially viewed kerosene LODs are improved relative to those obtained by radial viewing, but are degraded relative to an aqueous solution by up to one order of magnitude. The performance of this type of plasma using a mixed gas $Ar-O_2$ would be of interest.

7.3. Direct coupling of the plasma

LaFreniere et al. [25] used a He-purged direct plasma–spectrometer interface for the detection of Br, Cl and other analytes employing VUV spectral lines and axial viewing. With USN, the LODs were 8 $\mu g\,l^{-1}$ for Br and 15 $\mu g\,l^{-1}$ for Cl. The LODs of the VUV spectral lines of Al, Ga, and In were superior to those typically observed in the UV spectrum. A list of prominent emission lines and LODs of Al, As, B, Bi, Br, Cl, Ga, Ge, I, In, P, Pb, S, Sb, Se, Si, Sn, Te and Tl was provided (reproduced in Table 3). Calibration curves were linear over four orders of magnitude of concentration. The F I 95.2 and 95.5 nm resonance lines

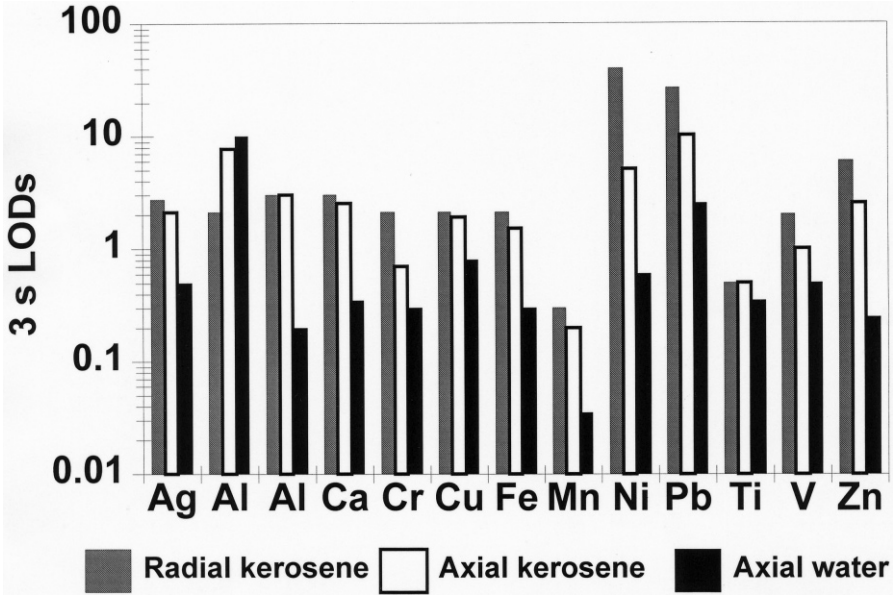

Fig. 6. Comparison of limits of detection (3 s $\mu g\,l^{-1}$) in kerosene and aqueous solution using axially and radially viewed ICPs. Data for aqueous solutions are from Table 3. Kerosene values are from Greb and Leitken [77].

Table 3
Prominent vacuum UV emission lines (< 180 nm) and LODs ($\mu g\ l^{-1}$) of emission lines observed using an end-on He-purged direct plasma–spectrometer interface[a]

Element	Wavelength (nm)	Pneumatic nebulizer	USN
Al II	167.08	0.4	0.04
Bi II	143.68	200	3
Br I	154.07	50	8
Cl I	134.72	50	15
Ga II	141.44	9	0.8
Ge I	160.26	60	4
Ge II	164.93	40	2
I I	178.22	20	6
In II	158.64	4	0.5
P I	177.50	15	3
Sb II	156.55	100	10
Se I	153.04	60	9
Pb II	168.22	25	2
Si II	153.34	30	2.5
Sn II	147.50	30	3
Te I	170.00	30	5

[a] Data reproduced from LaFreniere et al. [25].

could not be verified due to the presence of intense H I and N I lines.

LaFreniere et al. [26] used a direct injection probe (DIP) and an extended torch to introduce gaseous mixtures of Cl, Br, C, and S. The optimum end-on viewing position of the plasma was found to be approximately 3 mm off-axis. LODs were determined using a mixture of SF_6, Freon 12 (CF_2Cl_2) and Freon 13B1 (CF_3Br) in argon. The absolute LODs for Br I 154.07, Cl I 134.72, S I 180.73 and C I 165.7 nm were in the sub$\mu g\ l^{-1}$ range (0.2, 0.3, 0.006 and 0.1, respectively). These LODs surpass values for near infra red (NIR) spectral lines by 2–3 orders of magnitude. The fluorine resonance lines at 95.2 and 95.8 nm were observable when SF_6 was introduced into the axial channel of the plasma via the DIP. However, the emission of these lines was too weak to have analytical utility. The enhanced LODs were attributed mainly to the higher sensitivities of these VUV lines, the efficient optical sampling and the DIP mode of sample introduction. In the Spectro EOP instrument the LODs are 0.2 for Br I 157.484, 0.05 for Cl I 134.72, and 0.01 $mg\ l^{-1}$ for I I 142.5 nm (Table 3).

7.4. Secondary discharges and the Mach disk

Extracting the axial column of an ICP into a small vacuum chamber causes a secondary discharge [8,29]. A water-cooled orifice in a sampling cone was immersed in the axial zone of the plasma. Under the same ICP operating conditions, the intensities in a 40-MHz plasma were higher than those of a 27-MHz discharge. Analyte background spectra were similar to those observed in the ICP alone. The intensities of 13 ion lines observed in the secondary discharge were higher than those observed in the ICP alone. High energy potential (> 9 eV) atom lines were also enhanced but to a smaller degree. Low energy potential atom lines and those of the EIEs were suppressed. For example, the relative intensities of the ion lines of Mn, Zn and Cu were enhanced up to 10-fold, whereas Mn atom lines were relatively depressed by up to 50%. In comparison to the LODs quoted by Winge et al. [92], the LODs of the secondary discharge were improved by a factor of 3 or more. Houk surmised that LODs might be further improved by centering a skimmer on the axial channel as described by Montaser and Fassel [23]. This would remove the absorbing fringe of the ICP and allow the analyte-laden axial channel to flow through the skimmer into the discharge. The intensity enhancements observed were attributed to plasma constriction thus increasing the number density, the excitation temperature and the degree of ionization. Consequently, high-energy potential lines would be enhanced while neutral atom lines would be suppressed. It was concluded that atomization, excitation and ionization processes are more efficient in the discharge than in the plasma.

Houk and co-workers [32,33] described studies of the emission in the Mach disk region when the axial column of a 40-MHz ICP was extracted into a small quartz vacuum chamber through a small orifice in a water-cooled Cu-plate. The emission was measured with a Perkin Elmer Optima 3000 SCD spectrometer. In the vacuum chamber, a dark 'zone of silence' was surrounded by a concentric barrel shock wave called the 'Mach disk'. The intensities in the 'zone of silence' were low, increasing to a maximum 7 mm from the orifice,

which corresponds to the 'Mach disk'. The intensities in this region were lower than those observed in a conventional ICP by factors of 100–1000. The attenuation of ion lines was greater than those of neutral atomic lines. It is clear that the analytical potential of this configuration is limited unless considerable intensity boosting can be achieved.

7.5. Effect of aerosol flow rate

According to Brenner et al. [36], LODs of hard ion and atom lines, for example, As I 189.042, As I 193.759, Si I 212.412 and Cd II 226.502 nm, were improved in the axially viewed ICP when the aerosol flow rate was low. Whereas SBRs of 'soft' lines such as Al I 396.152 nm and K I 766.49 nm were enhanced at high flow rates. It was concluded that these nebulization-induced enhancements can be used to advantage for specific applications, for example, for the determination of low $\mu g\ l^{-1}$ Al concentrations in environmental and biological materials using high aerosol flow rates. In that study the good correlation of net line intensities and LODs with aerosol flow rates and excitation and ionization potentials was attributed to changes in temperature and energy conditions in the plasma as explained by Mermet [43,49,50]. Brenner et al. [36] also showed that the %R.S.D.s of analyte signals varied with aerosol flow rate, decreasing from 1.5 at 0.6 l min^{-1} to approximately 0.1–0.4 at 0.8–0.9 l min^{-1}.

7.6. Effect of RF power

Brenner et al. [36,37] measured the effect of power on net signals and SBRs of an axially viewed ICP. At constant aerosol flow rate, the net signal of Y II 371.0 nm increased with increasing power by a factor of 3. However, SBRs decreased by a factor of 6. This behavior was typical of other spectral lines studied. It was concluded that lower RF power for trace element determinations is more favorable, providing the plasma is sufficiently robust (Mg II/Mg I > 8) (see Mg II/Mg I section) [36]. However, LODs of high energy potential lines, for example, As I 188.979, 193.696 As I 188.98, Tl I 190.800 and Se I 196.026 nm were improved when the RF power was increased from 1 to 1.35 kW. [37].

8. Linearity

There are conflicting results on the linear dynamic range of axially viewed ICPs. Demers [12] directed a shear flow of air toward the apex of the plasma, and observed similar linearity ranges for axial and radial configurations. Nakamura et al. [39,45] using an echelle spectrometer with wavelength modulation and second-derivative detection reported a dynamic range of measurement that was linear over several orders of magnitude. Dubuisson et al. [35] reported that the dynamic range was reduced. It can be reasonably assumed that in those cases where non-linearity has been reported, the peripheral cool, absorbing fringe may not have been effectively diverted.

9. Interferences

While detection enhancement is important for trace element determinations in biological, environmental and geological samples from the above discussion, the use of axially viewed ICPs may not be straightforward for the analysis of these types of samples. This is due to changes in excitation conditions in the plasma caused by the presence of high concentrations of alkali and alkali earth elements in the solutions, which are then viewable with axial observation.

In all recent publications on the analytical characteristics of axially viewed ICPs, attention has been focused on comparisons of interference effects with radially viewed ICPs. Attention has also been given to the interferences observed in axially viewed ICPs with low and high aerosol loading (microconcentric, and conventional nebulization vs. USN and desolvation, respectively). In all the studies, several concerns are addressed:

1. What is the magnitude of EIE, Ca and acid interference effects in axially viewed plasmas.
2. Are the interferences larger or smaller than

those observed in radially viewed configurations?
3. What are the optimum ICP operation conditions for multi-element analysis — i.e. lowest LODs and minimum interference effects?
4. What is the relationship of the interferences and the energy potentials of the spectral lines and aerosol generation and transport mechanisms?

9.1. Effect of EIEs and Ca

In an early publication [85], on EIE interference effects in axially viewed ICPs the effect of Na on the intensities of various spectral lines was compared to a conventional radially viewed ICP. Cr ion and atom spectral line intensities decreased by approximately 25% in the presence of 5000 mg l^{-1} Na using a robust radially viewed plasma (an end-on sheath gas was employed). Signal suppression with axial viewing was only approximately 5% larger, implying that the differences between the configurations were small with respect to Na. This was an important conclusion since it indicated that under certain ICP operating and instrumental conditions, the analytical performance of axially viewed ICPs is similar to those of radially viewed plasmas.

Dubuisson et al. [35] measured Na matrix effects with axial viewing for several commercially available instruments. They found that the interferences were similar to those observed with radially viewed ICPs when the RF power was high, the argon carrier gas flow rate was low and the diameter of the torch injector was large (>2 mm); i.e. when energy transfer from the surrounding plasma to the central channel was optimum.

Brenner et al. [36] compared Na and Ca induced interference effects in axially and radially viewed ICPs. The effects caused by solutions containing up to 0.1% Na and 0.1% Ca on ion and atom line intensities of 15 element wavelengths differing in energy potentials were examined using a Varian Series II sequential spectrometer. They observed that matrix effects (expressed as the recovery of the various analytes based on a calibration using a multielement spike in 2% HCl) increased with increasing Na and Ca concentrations. Ca and Na effects with axial viewing were generally small (0.9–0.8) and were similar to those obtained with radial viewing. Indeed, effects with axial viewing were smaller than those observed with radial viewing (the closer the value to 1, the smaller the effect). They showed that Ca interference factors exceeded those for Na. This behavior was attributed to the robust plasma as evidenced by high Mg II/Mg I intensity ratios.

Brenner et al. [37] also investigated the effect of 0.1% Na and Ca in an axially viewed ICP using a CFN. A large diameter torch injector was employed. CFN Na interference factors for spectral lines of intermediate energy potential varied mostly from approximately 0.9 to 1.0, whereas CFN Ca effects were larger and varied from approximately 0.75 to 1.1 The emission intensities of low and high energy potential lines were enhanced and attenuated respectively, to larger degrees. Brenner et al. [44] measured the interference effects of 0.5% Ca and 0.5% Na and mixed Ca–Na solutions in axially and radially viewed ICPs. In the axial configuration, intensity suppression varied from 0 to 40%. In the radially viewed configuration, the interferences were smaller and varied from 5 to 15% for Na and from 10 to 30% for Ca. In both configurations, interferences increased with increasing Ca and Na concentrations. In the Spectro EOP [77], the intensities of Cd 226.502, Ni II 231.604 and Ti II 334.941 were reduced by 50% in the presence of approximately 8% Ca at 1.2 kW. In the presence of 1% Ca the signals were diminished by 20%. These observations are in contrast to various reports describing substantially larger interferences in the axial configuration than those observed in radially viewed systems. For example, Ivaldi and Tyson [34] showed that a high concentration of Na resulted in a large suppression by 65% (relative to an aqueous solution) of the analyte intensities. This was accompanied by a large decrease in plasma robustness reflected in the sharp decrease of the Mg II/Mg I nm ratio from 5.9 to 2. These values were obtained using a narrow torch injector and a Perkin Elmer Optima 3000 XL.

Of considerable interest are the results of De

Loos-Vollebregt et al. [16]. They evaluated K and Ca interferences in a low-flow water-cooled ICP. In the conventional radially viewed ICP, intensities decreased markedly above 1 g l^{-1}. In contrast, in the low-flow water-cooled ICP, intensities remained constant up to concentrations as high as 10 g l^{-1}. The remarkable reduction of interferences was explained by the spherical shape of the plasma and by the deflection of the cool plasma fringe convection.

While an average 10-fold LOD improvement can be attained using a USN with low salt concentrations, its use may be limited for the analysis of real samples where high concomitant concentrations can cause large variations in emission intensities [93]. According to Brenner et al. [36], the depressive effects of a 0.1% Na using a USN, in a robust axially viewed ICP, amounted to no more than 10%. When Cd II 226.502 nm was employed as an internal standard this effect was reduced to 2–3%, and the coefficients of variation were $<1\%$.

Brenner et al. [37] compared the effects of normal and high Na and Ca aerosol loads by aspirating 0.1% solutions with a conventional CFN and a USN. The emission intensities of various ion and atom lines differing widely in energy potentials were measured using a Perkin Elmer Optima 3000 XL SCD. The diameter of the central torch injector was 2 mm. In contrast to the 10 and 25% intensity suppression observed with conventional nebulization mentioned previously, interference factors of spectral lines of intermediate energy potentials were depressed to larger extents — from +25 to −30% for Na and −50 to +30% for Ca, respectively. The emission of low and high-energy potential lines were respectively enhanced and suppressed to larger degrees, especially in the presence of Ca. For example, the emission intensities of Be II 313.042 and 313.047 (13.26 eV), Cd II 226.502 (14.46 eV), Co II 238.892 (13.46 eV), Ni II 221.647 and 231.604 (13.66 and 14.02 eV) and Zn II 202.548 and 206.200 (15.51 and 15.4 eV) were suppressed by 50%. The intensity of Se I 196.026 (16.07 eV) was suppressed to a larger degree (60–80%). On the other hand, emission signals of Cu I 324.754 and 327.396 nm, Mg I 285.213, Pb I 216.999 and Li I 670.781 and Sr II 407.771 and 421.552 nm were enhanced by a factors amounting to approximately 2.5 particularly in the presence of Ca. Several atom and ion lines were not significantly effected, for example, Cd I 228.802, Fe II 238.204, 239.562, Ni II 232.003 and Zn I 231.856 nm.

De Wit and Blust [94] compared the effects of 1 and 3.5% NaCl in a Varian Liberty axially viewed ICP using conventional Meinhard concentric nebulizer and a low-consumption MCN. With the conventional concentric nebulizer, signal depression was approximately 30% for 0.9% NaCl and 45% for 3.5% NaCl. With the MCN, intensity reduction was significantly less — approximately 20 and 25%, respectively. This is probably due to the smaller amount of aerosol particles injected into the plasma. LODs for the MCN were generally higher than those for the concentric nebulizer.

Dubuisson et al. [48] adopted an alternative approach to explain Na induced interference effects in an axially viewed robust ICP. They investigated the role of the aerosol generation and transport system. They employed a Perkin Elmer Conespray nebulizer–cyclone spray chamber (CSN–CSC) and a cross flow nebulizer–double pass spray chamber (CFN–DPSC) to aspirate a 1% Na solution in the form of NaCl. The total solvent mass transported through the sample introduction device was determined by measuring the absorption of the aerosol and water vapor on silica gel at the exit of the spray chamber with and without 1% Na. In the presence of Na, the intensities of five ion lines varied from 70 to 90% of the signal obtained from a pure aqueous solution in a radially viewed ICP. Only 10% of the signal suppression was attributed to the difference in solvent transport rates. Consequently, it was concluded that aerosol generation did not have a notable influence on the Na effect. However, in the presence of Na the diameter of the DPSC tertiary aerosol droplets was smaller than obtained with a CSC (1.6 vs. 2.3 μm Sauter mean diameters, respectively). In a pure aqueous solution, a significant enrichment of the analytes was observed in the larger droplets (10–15% of the initial aqueous solution for the CSN–CSC combination and 10–25% for the Na solution). These

differences were attributed to a process similar to aerosol ion redistribution (AIR) described by Borowiec et al. [95]. However, it should be noted that interferences in the axially viewed ICP were greater than those of the radially viewed plasma (65–70% of the signal obtained in an aqueous solution for the CSN–CSC combination). This fact was not considered by Dubuisson et al. [48].

9.2. Acid effects

Acid interference effects in the ICP have been attributed to several sources: the aerosol generation and transport system due to decreased solution uptake as a result of increased viscosity [96,97], changes in the primary and tertiary aerosol drop size distribution [98] and changes in atomization and excitation conditions [99–103]. Dubuisson et al. [40] and Novotny et al. [70] compared the effects of acetic acid on the emission in axially and radially viewed ICPs. They demonstrated that the interference level was similar when the plasmas were robust. Dubuisson et al. [40] showed that under such conditions, spectral lines differing in energy potentials were affected to the same extent. A residual effect was attributed to physical interferences in the aerosol generation and transport system. Limits of detection were also substantially degraded in the presence of concentrated acetic acid [77] (Fig. 5). Signal suppression due to HCl and HNO_3 up to 10% concentration was 6% greater than in the radial system. Recoveries using axial viewing were improved using an internal standard [103].

Todoli et al. [82] also studied the acid interference effects of 0.9 and 3.6 M HNO_3 and H_2SO_4 in an axially viewed ICP. Three different types of nebulizers were studied: a MCN (Cetac Technologies, Omaha, NE, USA), a conventional Meinhard concentric nebulizer (TR-30-K2, Meinhard Associates, Santa Ana, CA, USA) and a Conespray nebulizer (Perkin Elmer). The MCN nebulizer is capable of aspirating liquids at several tens of $\mu l\ min^{-1}$. The emphasis of the study was on aerosol droplet distributions. The primary and tertiary aerosol drop size distributions were measured for liquid flow rates ranging from 0.03 to 0.6 ml min^{-1}. Primary aerosols originating from nitric acid were similar to those of water. Primary and tertiary aerosols produced by the MCN were finer than those produced by the other nebulizers. Unfortunately, matrix effects (expressed as the ratio of SBRs in acid to SBRs in water) were not directly compared with those observed in radially viewed ICPs. Furthermore, the low Mg II/Mg I ratios of approximately 6 indicated that non-robust plasma conditions prevailed, as a result of the aspiration of these acids. Todoli et al. [82] nevertheless concluded that variations in SBR were due to ionic redistribution phenomena in the spray chamber and not to a change in the excitation conditions in the plasma.

9.3. Effect of ICP operating conditions on matrix effects

The effect of operating conditions (RF power, observation height, aerosol flow rate, and desolvation) and EIEs on ionization, excitation and solute vaporization effects in radially viewed ICPs has been well documented [6,42–44,49,50,56,58,67–70,104–111]. In these investigations, it was observed that optimizing the RF power and the carrier gas flow rate reduced these interference effects. For example, Thompson and co-workers [104,105] demonstrated that increasing the forward power reduced Ca interferences. Dubuisson et al. [35] and Brenner et al. [37] studied the influence of RF power on Na and Ca interference effects in axially viewed ICP configurations. Interference effects were reduced at high RF power. Brenner et al. [37] compared the magnitude of the interference effects using normal and high aerosol loading. Increasing the RF power from 1 to 1.35 kW generally reduced matrix effects. In the case of Ca using a USN, an increase of power had a great effect on the high-energy potential lines the net emission signals of which increased by up to 30%. Interference effects on intermediate energy potential lines changed by approximately 10%, while low-energy lines were not significantly affected. The percentage change in the interferences on ion lines having energy potential sums varying from 10 to 18 eV were significantly correlated with their energy potentials. Brenner et al. [44] observed that interference effects caused

by 0.5% Ca and Na were attenuated when the RF power increased from 1.2 to 1.5 kW. The general trend of mixed Na–Ca solutions was similar to that of the individual concomitants. The Mg II 280.270 nm intensity increased significantly when the RF power increased, whereas, the emission change of Mg I 285.213 nm line was insignificant. This had an important effect on the Mg II/Mg I intensity ratio. This power effect was also observed by Romero et al. [69].

9.4. Relation of interferences with energy potentials

In general, the good correlation between EIE and Ca interferences and energies of the spectral lines, defined for radially viewed ICPs [104,105], was also observed in axially viewed ICPs [34–37] particularly in the presence of Ca [44]. In axially viewed ICPs, it has been shown that high-energy potential lines are more susceptible to interference [34–37]. Suppression of high-energy potential lines has been attributed to energy withdrawal from the plasma, required to atomize the high concentrations of Ca and Na. This process is accompanied by a decrease in excitation temperatures and consequent reduction in plasma robustness indicated by the decrease of the Mg II/Mg I intensity ratios [36,37] (see Section 6). However, the relation with Na is less pronounced and other processes have been invoked to explain variations of line intensity with increasing Na concentrations [38,83]; e.g. changes in the quality of the tertiary droplet sizes.

The close association of Ca-induced interferences and energy potentials of the spectral lines might be useful to predict interference factors in the analysis of geological and environmental samples [44] (see Section 9.6).

9.5. EIE effects in slurries

O'Hanlon et al. [112] studied effects of EIEs (Li, Na, K, Cs) on the intensities of atom and ion lines of Mg in solutions and in slurries in an axially viewed ICP. In the presence of EIEs, both atom and ion line intensities were enhanced in the order Li < Na < K < Cs. Ion lines were more affected than atom lines. In slurries, the amount of enhancement was less than in Na and Li solutions owing to the reduced atomization efficiency.

9.6. Internal standardization

Internal standards have been used widely to improve accuracy and precision by compensating for variations in the aerosol generation and transport systems, in the plasma owing to changes in atomization and excitation conditions, and drift due to thermal variations in the spectrometer itself. Internal standardization has also been applied to correct for the EIE and alkali earth element effects. The basic principles of internal standardization were outlined by Belchamber and Horlick [113] and Barnett et al. [114]. In the simplest circumstances, a single internal standard (e.g. Sc II, Y II) has been shown to compensate for variations due to salt and acid interference effects [41,42,71,115–119]. Mermet and Ivaldi [71], used real-time internal standardization employing a Perkin Elmer Optima SCD ICP spectrometer. They showed that if the differences in spectral line responses are small (when the plasma is robust and when the range of ionization plus excitation energies is small), a single internal standard line can be effective in improving the precision. Threefold improvements in precision were observed with simultaneous internal standardization, when the analytical signal was limited by flicker noise. Improvement factors of 50 were obtained in a radially viewed ICP for drift-derived variations. Precision values of 0.1% R.S.D. were obtained using a SCD-based spectrometer and axial viewing.

Ivaldi and Tyson [41] using real time internal standardization with an axially viewed ICP, observed that emission signals could be correlated with each other to a high degree for pure aqueous solutions and solutions containing 200 mg l^{-1} Ca and 100 mg l^{-1} K. They used a 1.45-kW ICP and an aerosol flow rate of 0.7 l min^{-1}. R.S.D.s were improved by a factor of 3–4 when Y II 371.030 nm was employed as an internal standard. Compensated ion line R.S.D.s were approximately 0.1–0.2%; the improvement of the atom lines was not as good, R.S.D.s varying from 1.5 to 3%.

Romero et al. [119] also applied the internal standard procedure in the sequential mode using a Varian Liberty 220 scanning spectrometer. Dubuisson et al. [42] demonstrated that a single internal standard (Ni II 231.604 nm) could be effective in compensating for Na-induced ionic spectral line suppression in a robust axially viewed ICP. It was concluded that variations, originating in the sample introduction system, could be compensated using this procedure. An attempt to compensate for the variable effects of Na and Ca in robust axially viewed ICPs was made by Brenner et al. [36] using Sc II 361.384 nm, measured sequentially, as the internal standard. For spectral lines similar in energy potentials, a significant improvement of *accuracy* was obtained. Whereas uncompensated recoveries varied from 78 to 92% for spiked Na and Ca solutions, compensated recoveries varied from 92 to 110%. Thus, a maximum negative bias of up to approximately 20% was reduced to $<10\%$. This partial compensation was due to the different responses of the analyte spectral lines in response to varying Na and Ca concentrations. Of interest is that, although the extent of compensation is maximum using simultaneous multielement spectrometers, the internal standard was also applied in the sequential mode by Brenner et al. [36] for the determination of major and trace elements in geological samples.

It is clear that several internal standard spectral lines are required to compensate for line variation in axially viewed ICPs. In the parameter-related internal standard method, two internal standards (Cd and Rb) were monitored by changes in the intensities induced by variations in RF power and sample uptake in a radially viewed ICP [104,105,120]. Matrix effects due to Na, Ca and Na–Ca matrices were studied for the determination of selected elements using Sc and Y as internal standards [121,122] using an USN. For solutions containing up to 80 mg l^{-1} Ca and Na, up to 25% depression in the signal was observed. Correction for matrix effects using the internal standard ratio method reduced the matrix effects to approximately 9%. Brenner et al. [37] studied the interference effects of 0.1% Ca and Na in an axially viewed ICP (Optima 3000 XL SCD), using conventional nebulization and an USN. At 1.35 kW, variations for ion lines were small. When Tl II 190.800 (12.60 eV) was used as the internal standard for compensating effects on spectral lines varying from 10 to 13 eV, uncompensated recoveries of approximately 90% were markedly improved to approximately 98–100%. A similar result was obtained for the high-energy potential lines using Be II 313.042 nm (13.28 eV) (see Table 3 in Brenner et al. [37]). However, in the case of the USN, more than two internal standards would have to be used (see Fig. 3 in Brenner et al. [37]). It was concluded that the magnitude of compensation in axially viewed ICPs as in radially viewed configurations, depends on the similarity of the energies of the analyte and internal standard spectral lines.

De Boer and Velterop [121] investigated matrix effects of Na and Ca in radially and axially viewed ICPs. They developed a proportional correction procedure to compensate for effects of 2000 mg l^{-1} Na and 400 mg l^{-1} Ca using a several internal standard Y and Sc ionic lines. In this routine, the effect on the analyte was brought into fixed relation with the effect observed for the internal standard. Matrix effects of approximately 20% were compensated to $<4\%$ when applying this procedure. The method was suitable for both single- and mixed-matrix component systems.

Brenner et al. [44] investigated interference effects of 0.5% Ca and Na and mixed Ca–Na solutions in an axially viewed ICP for ionic and atomic spectral lines varying widely in energy potentials using sequential and simultaneous spectrometers (Jobin Yvon-Horiba). They found that there was a close relationship between interference effects and energy potentials of the spectral lines studied. These linear correlations between Ca and Na matrix effects were estimated using atomic and ionic lines of Be, Sb, Sc and Y only. Whereas, analyte recoveries from 0.5% Ca and Na solutions varied from 40 to 90% without compensation, variations were $\pm 5\%$ for all atomic and ionic lines measured. The good linear correlation between the magnitude of interference effects and energy potentials of the spectral lines offers the possibility of applying variable compensation factors based on the energy potential of

the analyte wavelengths and interpolated interference factors. Such functions could be established by measuring the interference factors of four internal standard wavelengths that cover the range of the analyte energy potentials. Maximum compensation might be achieved by using a generalized internal standard method as described by Lorber et al. [123,124].

9.7. Skimmed plasma

Montaser and Fassel [23] showed that solute vaporization interferences ($Ca-PO_4$) were similar to those of conventional radially viewed plasmas. On the other hand, 1% Na resulted in increases of the Ca atom line by a factor of 3.

9.8. Direct coupling for VUV detection

The direct coupling of the plasma to the spectrometer for the detection of analytes using VUV spectral lines [24–26] presents a special case from the point of view of EIE interferences. In this configuration the axial channel of the ICP was viewed end-on using a direct plasma–spectrometer coupling interface via a He-purged water-cooled Cu-metal orifice. In general, it was noted that the insertion of this optical probe into the ICP for optical detection did not result in more extensive and complex interferences than those reported for ICP-MS.

LeFreniere et al. [25] reported that Br, Cl and Al VUV lines were not strongly affected by high concentrations of Na. The Ca interference on Al and vice-versa was similar to that described for UV spectral lines using radially viewed ICPs. The intensity attenuation of Al I 167.081 nm by 1000 mg l^{-1} Ca was 20% of that observed for an aqueous solution. With an USN the emission signal was suppressed by 90% for a 4000-mg l^{-1} Ca solution. In the presence of approximately 8 g l^{-1} Al, the Ca II 184 nm line was depressed by 15% using conventional pneumatic nebulization, and 50% using USN and 2.7 g l^{-1} Al. It was also observed that the matrix effect on the Ca II 184 line was greater than the Ca II 393.4 nm line.

10. Applications and techniques

10.1. Geoanalysis

Although geoanalysis using ICP-AES is now well established and documented [56,115,118, 125–127] and the technique is rapidly approaching maturity, the data describing the merits of axially viewed ICPs is limited for this application. Brenner et al. [36] evaluated the analytical performance of axially viewed sequential ICP spectrometers (Varian Liberty 220 and Series II). Precision and accuracy was improved when Sc II 361.384 nm, as an internal standard, was measured sequentially. The procedure was validated by analyzing standard geological reference materials (SRM) [128] for major, minor and trace element contents. Samples were decomposed using a sodium peroxide sintering procedure [129]. A sample weighing 0.5 g was sintered with 2.5 g sodium peroxide in a Zr metal crucible for 45 min at approximately 500°C. The fused cake was dissolved in hydrochloric acid (1:1 v/v) and made up to 100 ml. The correlation coefficients, describing the goodness of fit and the concentration ranges were summarized. In all cases, calibration accuracy improved with internal standard compensation. Since the presence of large amounts of Na in solution might have had a 'buffering' effect in the plasma, most of the compensated variation was considered to be due to physical effects in the aerosol generation and transport system [36]. Calibration curves were linear for at least 3–4 orders of magnitude. Approximately 15 trace elements were determined sequentially together with major and minor elements with satisfactory precision and accuracy. The accuracy of major and minor element determinations in geological samples was evaluated using a simultaneous axially viewed ICP CCD spectrometer (Varian Vista) [130]. Samples were decomposed using a lithium metaborate fusion [129]. The accuracy was evaluated by analyzing several geological SRMs [128]. R.S.D.s were $<1\%$ for 5-s integration. A comparison of the determined values with the recommended data demonstrates that the accuracy was excellent. Owing to the enhanced LODs of the axially viewed

ICP, several trace elements were also determined with satisfactory accuracy. In these solutions the analytes were diluted 1000-fold with respect to the solid.

10.2. Agricultural samples

Raven et al. [131] used an axially viewed ICP and a Perkin Elmer SCD for trace element determinations in fertilizers and in soil amendments. Wastes, sludge, various phosphate compounds, natural phosphate rock, dolomite, ammonium sulfate and potassium chloride and magnesium potassium sulfate were digested in a microwave oven using a mixture of HNO_3–HF–H_2O_2–H_3BO_3. Di-ammonium phosphate, magnesium potassium sulfate and dolomite were decomposed with HNO_3 and H_2O_2. The final solutions were filtered through a 0.45-μm membrane. Calibration was performed with matrix-matched solutions. Accurate results were obtained for Ag, Ba, Be, Cd and Ni, and for As, Mn and V in the absence of high concentrations of Cr, Ni and Ti which were sources of spectral interference. LODs in the matrix-match solution varied from < 0.7 to 17 μg l^{-1}; these were significantly degraded in comparison to the values in Table 2 probably due to the high acid and salt concentrations.

10.3. Biological and clinical samples

Barnes [132] used an axially viewed ICP for the analysis of food products. Fruit pulp and juice were homogenized with HNO_3/H_2SO_4 (5:1) and the mixture digested in a microwave oven at 51–96 W for 24 min, cooled and diluted with 3 ml H_2O. The analysis was performed using an Optima 3000 DV SCD spectrometer with a nebulizer flow of 0.75 l min^{-1} and plasma gas of 15 l min^{-1}. Recoveries for various fruit beverages varied from 80 to 125%. The elemental composition was used for nutritional labeling, geographical source, tampering, and contamination.

Thiel and Danzer [66] analyzed wine using an axially viewed ICP and a conventional echelle-based PMT multichannel spectrometer (Maxim). Fifteen elements were determined in various types of wine. Calibrations matrix matched with ethanol, were generally linear up to 10 mg l^{-1}.

Montaser and Fassel [23] determined the Cr and Al concentrations in blood samples using an axially viewed ICP. The outer cool plasma fringe was rejected using a Cu-metal skimmer. Using the methods of addition and a 10-fold dilution, the Al and Cr concentrations were 80 and 25 μg l^{-1}, respectively.

10.4. Water analysis

Nakamura et al. [39,45] determined major and trace elements in the pristine NRCC CRM SLRS-2 Trace Elements in Water SRM using an axially viewed ICP and an extended torch. The comparison between determined and certified values was satisfactory. However, this test does not reflect the validity of their setup to determine trace elements in waters containing even moderate salt concentrations. Furthermore, sub μg l^{-1} concentration levels could not be determined. De Boer [124] employed an axially viewed Perkin Elmer 3000 XL spectrometer for the determination of Cr, Cu and Ni in groundwater.

10.5. Food analysis

Barnes [133] described the determination of trace elements in food. They used a 10-mg l^{-1} aqueous calibration standard which did not take into account the effect of the high concentration of sample concomitants on the efficiency of aerosol generation and transport and on the conditions of excitation and atomization. A high forward power of 1.45 kW was used. The memory effect was evidently large since 120-s wash out was required. Ryan [134] described the application of an axially viewed sequential ICP spectrometer for direct analysis of milk powder using aqueous calibration standards. A V-groove nebulizer was employed and the suspension was continuously agitated during aspiration. Triton-X-100 was used to improve the stability of the milk powder suspensions. A large amount of Cs (1%) was added to compensate for varying interference effects of Na, K and Ca. Differences in viscosity were compensated using Sc II 361.384 nm as the

internal standard. Sc also improved the long-term precision; the maximum deviation of approximately 10% was reduced to approximately 2%. The values obtained for NIST SRM 8435 Whole Milk Powder compared well with the recommended data.

10.6. Cosmetics

Besecker et al. [135] described a method for the analysis of cosmetic materials. Samples were partially decomposed using a microwave oven.

10.7. Polymers

Besecker et al. [136] developed a closed-vessel microwave digestion procedure for the analysis of high-density polyethylene, polystyrene and various polymer blends. A RF power of 1.36 kW and an aerosol flow rate of 0.7 l min^{-1} were used. Spike recoveries varied from approximately 85% for Pb using the high-energy potential line of Pb II 220.353 nm to 98% for low energy Mg II 279.553 nm.

10.8. Particulates and air pollution

Seltzer [137] described a unique application of an axially viewed ICP. The improved LODs were utilized with advantage for the determination of airborne hazardous metals. Optimum plasma operating conditions were employed for the determination of 14 elements. They listed optimum wavelengths and provided LODs in aqueous solution.

10.9. Speciation

Kato et al. [138] used an axially viewed ICP to determine methyl mercury by tandem capillary column gas chromatography using an axially viewed ICP.

10.10. Steels

Duffy and Thomas [83] described a method for the determination of B, P and S in low alloy steels. Steel samples weighing 1 g were decomposed with 20 ml of a solution prepared by mixing 0.2 ml Br and 5 ml HNO_3 and 15 ml H_2O, followed by 1 ml HF and 5 ml HCl. The final volume was 100 ml. B, P and S were determined using B I 182.527 nm, P I 178.221 nm and S I 180.669 nm. The RF power was 1.45 kW. Detection limits for axial viewing were 5–10-fold better than those obtained by radial viewing.

10.11. Analysis of NaCl brines

Fuxing et al. [17,18] employed an axially viewed ICP coupled to an optical quartz spectrograph for trace element determinations in NaCl brines. A specially designed bell-mouth nebulizer permitted the analysis of trace elements in NaCl for the caustic soda production. LODs for several trace elements in saturated brine varied from 0.003 to 0.2 mg l^{-1}. The recoveries from 6% NaCl at the mg l^{-1} level varied from 90 to 110%.

10.12. Nuclear materials

Fuxing et al. [17] used a quartz spectrograph with a linear dispersion of 0.35–11 nm mm^{-1}, a 27-MHz RF generator and an axially viewed ICP for multi-element analysis of various U compounds. The cool fringe of the plasma was rejected using a cross-flow of air. A tri-(2-ethylhexyl) phosphate poly-trifluoro-chloro-ethylene (TEHP-KEL-P) reversed-phase partition chromatographic column was employed to separate uranium from the trace elements which remained in the 3 N HNO_3 phase. The recovery varied from 84 to 118% with exception of K, Bi and Ta. The limits of determination were < 1 mg kg^{-1} with a sample weight of 200 mg.

10.13. Determination of the halides using VUV spectra lines

LaFreniere et al. [25] used a He-purged direct plasma–spectrometer interface and a solar blind PMT for determination of Br and Cl employing VUV spectral lines and axial viewing. With an USN, LODs were 8 $\mu g\ l^{-1}$ for Br and 15 $\mu g\ l^{-1}$ for Cl. Analytical calibration curves were linear over four orders of magnitude of concentration.

This interface was also used for the analysis of a gaseous mixture of Br, Cl, C and S compounds using a direct injection probe described by LeFreniere et al. [26]. LODs were 50, 80, 30 and 20 pg, respectively. The R.S.D.s were 2% or better.

10.14. Application of axially viewed ICPs in atomic absorption spectrometry (AAS)

The introduction of the ICP in the late 1960s as an efficient excitation and atomization cell for single and multi-element analysis was when AAS was at the height of popularity. The use of the ICP source was proposed as an atom reservoir for AAS by several investigators [10,139–141]. However, this approach stalled when Abdallah et al. [10] listed the disadvantages of ICP-AAS and radially viewed ICPs surged forward to become an analytical champion.

A series of papers by Rayson et al. [142–146] described the application of an axially viewed ICP for AAS, taking advantage of the cool absorbing fringe. The design of a special linear flow torch (LFT) and a data acquisition system for AAS determinations was detailed. This LFT configuration provided greater light output and higher signal-to-noise ratios than tangential flow torches (TFTs). Ag, Cu, Mg, and Ca were determined using a large coolant flow and a large sample introduction tube. The radiation from the hollow cathode lamp was directed through a fused silica lens and a so-called see-through torch. The aerosol was generated using a conventional concentric nebulizer and a Scott-type spray chamber. A time-gated data acquisition system using a boxcar averager was described. Time-gated data were obtained during time intervals of lower power input in the modulation cycle. 'Cool' plasma operating conditions were employed to maximize atomization and to minimize ionization in the plasma. LODs, which varied from approximately 0.2 to 10 $\mu g\ l^{-1}$ for Ag, Ca, Cu, Mg, and Au, were comparable to those obtained by ICP-AES. However, the linear dynamic range was only up to two orders of magnitude. EIE and solute vaporization interference effects due to Na and $NH_4H_2PO_4$ were determined. While it was shown that the LFT configuration produced less severe interferences due to Na than the TFT, these interferences resulted in an increase in absorption signals, which could be corrected by using an appropriate blank. The effect of the aqueous aerosol droplets on light scattering was evaluated. Desolvated aerosol droplets, plasma background and continuum resulted in an apparent increase in absorption due to non-specific radiation. For some elements like the rare earths, AAS determination using axial viewing was complicated by the intense atomic emission.

10.15. Direct solids analysis

Direct solids analysis using slurry nebulization, spark and laser ablation, and direct sample insertion, has numerous advantages namely minimum sample preparation, especially in the case of chemically resistant refractory materials (such as spinels, alumino-silicates, complex ceramics and alloys). For these types of materials, satisfactory recoveries can only be obtained by fusing the samples with lithium borate and sodium peroxide resulting in elevated blanks, interference effects in the sample introduction system and in the plasma. Moreover, volatile elements may be lost due to the high temperature of decomposition.

Direct solids analyses using plasma-based techniques were recently surveyed [147,148]. Notwithstanding the benefits of direct solids analysis, the number of publications describing the application of axially viewed ICPs using these advanced techniques is small. Using axial viewing, there is a potential for reduced matrix effects due to spatially controlled plasma-particle effects, since the region of observation in the plasma column is averaged due to the relatively large depth of focus.

10.15.1. Slurry nebulization

Slurry nebulization into radially viewed ICPs has been applied widely by several workers [149–156]. The main advantage of slurry nebulization is the low cost of a high solids V-groove nebulizer and a laboratory agitator necessary for delivering the suspensions to the plasma without clogging. Materials having sub micron particle sizes such as colloidal clay mineral suspensions

have been analyzed using aqueous calibration standards [152,155]. However, in the case of refractory silicate materials, the behavior of the suspended mineral particles in the plasma and in the aerosol generation and delivery systems is not similar to that of aqueous aerosols [149–151,153]. As a result of these diverse processes, analyte atomization efficiencies may vary widely and consequently quantification of refractory geological materials may not be easily attained. Basically, quantitative analysis can be attained when the transport of the slurry aerosols and their interaction with the ICP are identical to those of the calibration standards, or the differences are somehow compensated. Thus quantitative major, minor and trace element determinations have been made using matrix match calibration standards consisting of geological SRMs [151,153].

There are only a small number of publications describing the analysis of slurries using axially viewed ICPs [112,156]. Brenner et al. [156] aspirated geological SRM slurries prepared using the zirconia bead and bottle method [151–156]. A V-groove nebulizer was employed and emission signals were processed using a 0.75-m Czerny Turner sequential axial view spectrometer (Varian Series II). Data for several geological SRMs, prepared in an identical way are listed in Table 4. Comparison with the recommended values is satisfactory, indicating that axially viewed ICPs can also be used for the analysis of geological slurries.

10.15.2. Spark ablation

In spark ablation ICP-AES, a high-energy spark generator is utilized as a particle generator and the particulates formed by the electrical discharge are transported to the ICP via an argon carrier gas, where they undergo atomization, excitation and ionization [148,157,158]. Spark generators differ in the extent of surface melting vs. physical ablation processes. Graphite and tungsten rods are used as counter electrodes.

Although the application of spark ablation using radially viewed ICP-AES has been widely employed for direct solids analysis of metals and alloys [157,158] and non-conducting materials [153,161] prepared by pressing the powders with a conducting binder (Cu, graphite) the utilization with axially viewed ICPs is limited. Gagean and Mermet [160] compared spark ablation and UV excimer laser ablation (LA) for analysis of metals and alloys using an axially viewed ICP coupled to a polychromator (TJA Solutions 61E). A standard TJA Solutions spark ablation device was used. The pre-ablation time was brief, amounting to 20 s. Integration times were either 1 or 10 s depend-

Table 4
Slurry analyses of geological SRMs using a Varian Series II axially viewed ICP [156][a]

	Wavelengths (nm)	MAG-1 Det	MAG-1 Rec	SO-2 Det	SO-2 Rec	NIST2704 Det	NIST 2704 Rec
Wt.%							
TFe_2O_3[b]	259.940, 259.837	7.1	6.8	8.1	7.89	6.15	5.88
Al_2O_3	308.215	16.1	16.37	14.4	15.0	11.9	11.54
CaO	317.933, 315.887	1.4	1.37	2.85	2.77	3.5	3.64
MgO	279.079, 280.270	2.9	3.0	1.0	0.89	2.18	1.99
TiO_2	334.941, 337.280	0.75	0.75	1.48	1.43	0.8	0.76
MnO	257.610	0.1	0.098	0.10	0.09	0.07	0.072
mg kg $^{-1}$							
Ba	233.527, 455.403	483	479	1150	1000	400	414
Cr	267.716	115	97	18	12	125	135
Sr	407.771, 421.552	155	146	330	331	145	130

[a] Certified SRM data are according to Govindaraju [130]. 1.2 kW, integration time 0.5–1 s. Aerosol flow 0.7 l min^{-1}. Mg II/Mg I ratios were 9 ± 1. Calibration was performed using USGS Shale SCO-1, NIST 1633a fly ash, and USGS AGV-1. Si 251.412 nm and 288.158 nm were used as variable internal standards. Rec — recommended value; Det — determined value.

[b] TFe_2O_3 — total Fe as Fe_2O_3.

ing on signal intensity. Ablation efficiency and sensitivity expressed as SBR, was determined for cast iron, steel, bronze, brass, Zn alloys, aluminum, Cu–Al alloys and Pb metal. Ablation efficiency depended on the type of material and signal variations could not be compensated using a single internal standard element. Cast iron and steel were among the materials that were most difficult to ablate. The analytical ablation time was shorter for spark ablation than for laser ablation because less surface preparation was required. Spark ablation is the preferred technique for bulk analysis in terms of cost and analytical performance.

Brenner and Zander [161] used the Varian Vista CCD axially viewed ICP for the analysis of silicate rocks. Using similar spark and ICP conditions established in a previous investigation [159], C-based pressed silicate rock pellets were analyzed for major and trace elements. The accuracy of the working curves was improved by employing Si I as a variable internal standard.

10.15.3. Laser ablation

Moenke [162,163] pioneered the development of laser ablation for bulk and local direct solids analysis. The method was reviewed by Darke and Tyson [164]. The cloud of ablated micro particles is transported to the ICP by a flow of argon gas, where the sample is dissociated, atomized and excited. The most common laser is a Nd-YAG laser operating in the UV; excimer lasers (XeCl, KrF) have also been used [164]. These systems are capable of ablating a small amount of solid material (ablated spot ~ 10 μm) with minimum matrix effects due to fractionation caused by matrix–laser beam interaction [165]. While the technique has become widely accepted for trace element determinations using ICP-MS, the main scope using radially viewed ICP-AES is major and minor trace element determinations using stationary beam focusing. The advantage of axially viewing would be the enhanced LODs for trace element determinations and the study of element distributions in zoned areas and inclusions by moving the stage while ablating the specimen. Calibration is usually performed using relative sensitivity factors and matrix match procedures using SRM glass and pressed pellets. Intrinsic and external internal standards can be used to compensate for variable rates of ablation and fractionation effects. In the case of local analysis, a major element predetermined by an SEM-analyzer or an X-microprobe can be employed.

Gagean and Mermet [160] compared UV excimer laser ablation and spark ablation (see spark ablation section) for analysis of metals and alloys using an axially viewed ICP coupled to a polychromator (TJA 61E). The laser system was a Lambda Physik LPX 110I 308 XeCl laser. The forward power of the ICP was 0.95 kW. The repetition rate was 10 Hz and the energy varied from 175 to 215 mJ. The ablated materials were transported to the axially viewed ICP via a standard cyclonic spray chamber normally used for pneumatic nebulization of solutions. A 5-min pre-ablation period was required owing to the large dead volume of the ablation cell. In order to obtain satisfactory R.S.D.s even larger pre-integration times were necessary. Ablation efficiency and sensitivity expressed as SBR, was determined for several types of materials. The position of the plano-convex focussing lens was optimum when maximum acoustic emission was obtained. Beam masking enhanced the coupling efficiency of the laser sample surface. LODs were determined using the 308-nm XeCl excimer laser that was operated at higher power. R.S.D.s for the background were $< 1\%$, similar to those obtained for aqueous solutions using the same ICP system. Axial viewing resulted in enhanced SBRs; LODs were significantly improved when compared to the values obtained by radial viewing. The average improvement factor was 5 for steel and 20 for Al. In comparison to previously reported data, these LODs compared well with those obtained by ICP-AES, direct current plasma-AES and ICP-mass spectrometry.

As in the case of spark ablation, laser ablation efficiency depended on the type of material. In particular, steel and cast iron samples were more difficult to ablate than other metal samples. Different ablation efficiencies could not be compensated using internal standards because SBRs for various analytes and for the same analyte differed in the various matrices; i.e. evidently fractiona-

tion effects were significant. For example, Mn as an internal standard only partially compensated for this effect. This process also limits the possibility of using one type of material as a calibration standard for the analysis of the other types of material. R.S.D.s were $< 1\%$, similar to those for aqueous solutions. LODs in the solid were in the sub-ppm range and were improved relative to those obtained by radially viewing by a factor of 5 for steel to 20 for Al.

Hammerlin et al. [166] employed a Perkin Elmer Optima 3000 DV SCD spectrometer in the axial mode for the analysis of additives in solid polyvinyl chloride (PVC). An UV Nd-YAG laser was used with a 2.5-mm beam mask to ablate solid particles into the axially viewed ICP. The energy range was 2–20 mJ. Accuracy was evaluated by analyzing six in-house PVC reference materials that were prepared by doping the elements of interest in increasing concentration. After a pre-ablation period of approximately 5 min, the emission of the analytes (Al, Ca, Mg, Na, Sb, Sn, Ti) remained constant for approximately 20 min. This indicated that the laser ablation and plasma atomization processes were stable over an extended period, and that the distribution of the analytes was homogeneous. The 3σ LODs for the excimer laser (in the mg kg^{-1} level) were superior to those attained using the Nd-YAG laser by factors of 1.5 to two orders of magnitude. These LODs are similar or better than those obtained using pneumatic nebulization. The accuracy of the analytical data was measured by analyzing the materials using ICP-AES, neutron activation analysis and X-ray fluorescence spectrometry. Satisfactory data were obtained for Al, Ca, Cd, Mg, Sb, Sn and Ti. The reproducibility varied from 2 to 5%.

10.15.4. Direct sample insertion

The application of direct solids insertion using a radially viewed ICP was described by Karanosios et al. [167]. Skinner et al. [168] evaluated the merits of an axially viewed ICP for direct solids analysis using direct solids insertion of graphite cups into an ICP. Thin-walled carbon cups were employed to enhance volatilization rates. One of the cup designs incorporated a hollow stem through which a halogenating gas, e.g. Freon 12, could be introduced in order to facilitate the vaporization of refractory constituents. SBRs using axial viewing were higher than those for radial viewing, and the Cu, Pb and Sn LODs (but not Zn), were improved using both peak-height and peak-area methods of acquisition.

10.15.5. ETV

Hassler et al. [169] used an axially viewed TJA Solutions IRIS CID spectrometer. Several ETV configurations were evaluated. Tube length and 'nozzle' design were optimized. Trace elements were determined in SiC, CaF and stream sediments. LODs varied from 0.05 to 0.5 ng for most of the analyte spectral lines studied. Schrön et al. [170] coupled an ETV to a Fisons Maxim axially viewed ICP for the direct solids analysis of powdered geological samples. Sample vaporization was enhanced by halogenation. The LODs for Cr, Cu, Ni, Pb, and Zn were in the 1–500-μg g^{-1} range.

11. Summary

ICP-AES would benefit from improved LODs. In particular, in environmental, biological and geo-analytical applications, toxic and low abundance elements seldom can be determined with radially viewed ICPs and conventional modes of sample introduction. With axial viewing, LODs are improved by factors varying from 2 to 20 and when enhanced sample introduction techniques are employed such as USN and thermospray, they are further enhanced by up to a factor of 30. However, for high salt solutions, LODs are degraded due to interferences from EIEs and the alkali earth elements owing to an increase in aerosol loading in the plasma causing changes in atomization and excitation conditions. LOD improvement factors using the USN are not uniform owing to the relation with energy potentials of the spectral line. The SBRs of low-energy potential spectral lines increase when the aerosol flow-rate increases and vice-versa. This can be explained either by a drastic change in the IRZ position,

resulting in a more favorable observation zone, or a change in excitation conditions.

While LODs are an important figure of merit, matrix effects due to low ionization potential EIEs and Ca in particular, are detrimental to analytical performance. These matrix effects have been correlated with the spatial distributions of ion and atom spectral lines in the NAZ. These patterns are the result of several processes such as nebulization, excitation, shifts in ionization equilibrium and collisional processes. Both intensity enhancement and depression, depending on the excitation and ionization energies of the analyte, concomitant element and the observation zone in the plasma have been reported. In radially viewed ICPs the addition of EIEs enhanced analyte emission in the lower region of the plasma, while depressing it higher in the plasma.

While spatial emission behavior can account for these interferences in radially viewed ICPs, spatial inhomogeneity may have less influence in axially viewed ICPs where the field of observation may be quite large. Davies et al. [107] showed that by using the correct optics, the spatial variations of soft and hard lines are essentially negated with axial viewing due to optical integration of emission from all regions of observation. Thus, one might expect that the observed interferences would be lower in axially viewed ICPs than in radially viewed plasmas and to a certain extent this has been observed in robust axially viewed ICPs.

As in radially viewed ICPs, the effect of Ca is significantly larger than that of Na and the magnitude of the effect is dependent on the energy potentials of the spectral line, higher energy lines exhibiting greater suppression, while the emission of low energy potential lines are enhanced. Numerous investigators have shown that there is a close correlation between excitation and ionization potentials of the analytes and lowering of excitation temperature and dissociation energies. Therefore, interference effects in the axially viewed ICP could be due either to a dramatic change in the position of the NAZ or/and energy withdrawal, accompanied by a decrease in excitation temperature required to dissociate and atomize the concomitant matrix and analytes. Indeed, there seems to be little difference in the level of interferences in robust plasmas regardless of the geometry of observation. However, it appears that not all axially viewed plasma configurations respond in a similar way to increasing concentrations of EIEs and Ca and varying ICP operating conditions. It is, however, clear that high power, optimum residence time and efficient energy transfer (a wide torch injector and intermediate aerosol flow rates) are of vital importance for the analysis of geological, biological and environmental materials.

In addition to power compensation, interference effects can be partially compensated by applying a single internal standard both in sequential or in simultaneous measurement modes. However, due to the variable responses of the spectral lines to variable EIE and Ca concentrations, in accordance with energy potentials, a satisfactory compensation is only obtained if the energies of the spectral lines are similar to those of the internal standards. Therefore, a comprehensive correction can be achieved only by using several internal standards differing in energy potentials. In this respect, energy potential–interference factor functions may be used to compensate for EIEs and Ca interference effects.

The Mg II 280.270 nm/Mg I 285.213 nm ratio is a useful tool for quantifying plasma robustness in response to changes in ICP operating conditions, solvent and aerosol load and composition. It appears to be one of the more important criteria for the evaluation of the performance of ICP atomic emission systems. Values vary considerably among the various commercial systems and for the same system when excitation conditions are changed. For similar conditions and sample composition, the ratios of axially viewed ICPs are lower than those for radially viewed systems. It has not been determined why this is observed.

In the axially viewed ICP, high Mg II/Mg I ratios (>8) and minimum EIE and Ca interference effects are probably the result of several inter-related factors:

1. The use of relatively wide torch injector tubes (>2mm). Narrow torch injectors result in degraded energy transfer. Mg II/Mg I ratios

might be improved by further increasing the diameter of the central torch injector, thus increasing the residence time, and energy transfer. High ratios are also obtained when the aerosol flow rate is approximately 0.5–0.7 l min^{-1}. This may also be related to the quality of the aerosol.
2. The use of high RF power ($>$ 1.5 kW) results in the increase of the ratio accompanied by a reduction of matrix effects. In this respect, the use of high RF power is favorable for the analysis of environmental and geological samples containing even moderate concentrations of EIEs, alkali earth elements and acid concentrations.
3. It seems that minimum EIE interferences coincide with Mg II/Mg I ratios $>$ 8.
4. The question of whether end-on gas dynamics has an advantage over the cross flow cut-off gas configuration cannot be answered until an experiment using both configurations is conducted using the same sample introduction system, the same RF generator and the same spectrometer.

With respect to direct solids analysis, axially viewed ICPs have several advantages:

1. Spatially controlled interference effects due to particle–plasma interactions [171,172], could be averaged because of the large depth of focus of the NAZ.
2. As a result of improved LODs, small localized areas and spatial studies can be performed using laser ablation.
3. Enhanced LODs can also extend the scope of spark ablation to include the determination of trace elements.

12. Conclusions

It is likely that the utilization of axially viewed ICP-AES for multielement analysis will increase. The challenge lies in maintaining the detection advantage while minimizing matrix effects. At present interference effects must be evaluated since not all instruments respond to the same extent, especially when high aerosol loads are aspirated. It seems that robust axially viewed ICPs can be used in a wide range of analytical applications, possibly overcoming the need for radial setups or for configurations having both axial and radial viewing capabilities.

Acknowledgements

I.B. acknowledges the financial assistance of Varian Instruments Inc, Palo Alto, CA, USA. The authors also wish to express their sincere gratitude to Professor Jean-Michel Mermet, University Claude Bernard, Lyon, France for his perpetual encouragement. Mermet has led the way in development of axially viewed ICPs and made an indelible impression on the application and understanding of the inductively coupled plasma using both atomic emission and mass spectrometry. The authors are grateful to the reviewers for their constructive comments. The impeccable review and editing of the manuscript by Dr. M. de Loos-Vollebregt and Prof. Mermet resulted in its substantial improvement.

References

[1] I.B. Brenner, P. Bremier, A. Le Marchand, Performance of an air-cooled USN and a 40 MHz RF generator, J. Anal. At. Spectrom. 7 (1992) 819.
[2] V.A. Fassel, B.R. Bear, Ultrasonic nebulization of liquid samples for analytical inductively coupled plasma-atomic spectroscopy, Spectrochim. Acta Part B 41 (1986) 1089–1113.
[3] J.A. Koropchak, D.H. Winn, Thermospary sample introduction for atomic spectroscopy, Trends Anal. Chem. 6 (1987) 171–175.
[4] M.T.C. De Loos-Vollebregt, J.J. Tiggelman, P.C. Bank, C. Degraeuwe, Thermospray sample introduction into a horizontal low-flow inductively coupled plasma with end-on observation, J. Anal. At. Spectrom. 4 (1989) 213–217.
[5] Z. Horvath, A. Lasztity, R.M. Barnes, Preconcentration and separation techniques for inductively coupled plasma atomic and mass spectrochemical analysis, in: I.B. Brenner (Ed.), Geoanalysis using Plasma Spectrochemistry. Spectrochim. Acta Rev. 14 (1991) 45–78.
[6] P.W.J.M. Boumans, J.J.A.M. Vrakking, Detection limits of about 350 prominent lines of 65 elements observed

in 50 and 27 MHz inductively coupled plasmas (ICP): Effects of source characteristics, noise and spectral wavelength, Spectrochim. Acta Part B 42 (1987) 553–579.

[7] M. Murillo, J.M. Mermet, Improvement of the energy transfer with added-hydrogen in inductively coupled plasma atomic emission spectrometry, Spectrochim. Acta Part B 44 (1989) 359–366.

[8] B.H. Lim, K.P. Carney, M.C. Edelson, I.B. Brenner, R.S. Houk, An extraction discharge source for inductively coupled plasma atomic emission spectrometry: spectral line widths and interference effects, Spectrochim. Acta Part B 48 (1993) 1617–1623.

[9] T.J. Burden, J.J. Powell, R.P.H. Thompson, Optimal accuracy, precision and sensitivity of inductively coupled plasma optical emission spectrometry: bioanalysis of aluminium, J. Anal. At. Spectrom. 10 (1995) 259–266.

[10] M.H. Abdallah, R. Diemiaszonek, J. Jarosz, J.M. Mermet, J. Robin, C. Trassy, Etude Spectrometrique d'un plasma induit par haut frequence, Anal. Chim. Acta 84 (1976) 271–282.

[11] F.E. Lichte, S.R. Koirtyohann, Induction Coupled Plasma Emission from a Different Angle. Pap. 26, FACSS, Philadelphia, PA, 1976.

[12] D.R. Demers, Evaluation of the axially viewed (end-on) inductively coupled argon plasma source for atomic emission spectroscopy, Appl. Spectrosc. 33 (1979) 584–591.

[13] G.R. Kornblum, 2nd ICP Conf., Noordwijk aan Zee. Excitation mechanisms — physical data, excitation models. Report by Danielsson, A., ICP Inf. Newsl. 4 (1978) 147–171.

[14] L.M. Faires, T.M. Bieniewski, C.T. Apel, T.M. Niemczyk, 'Top-down' versus 'side-on' viewing of the inductively coupled plasma, Appl. Spectrosc. 39 (1985) 5.

[15] J. Davies, J.R. Dean, R.D. Snook, Axial view of an inductively coupled plasma, Analyst 110 (1985) 535–540.

[16] M.T.C. De Loos-Vollebregt, J.J. Tiggelman, L. De Galan, End-on observation of a horizontal low-flow inductively coupled plasma, Spectrochim. Acta Part B 43 (1981) 773–781.

[17] P. Fuxing, Y. Suling, H. Quinghua, W. Xiaoping, M. Heying, H. Yanmin, X. Yuxin, Y. Xu, W. Tingfang, Determination of forty trace impurity elements in uranium compounds using inductively coupled plasma atomic emission spectrograph with end-on viewing of the ICP and a medium-size spectrograph, Spectrochim. Acta Part B 41 (1986) 1211–1216.

[18] P. Fuxing, Y. Suling, H. Quinghua, K. Daming, X. Yuxin, Direct determination of trace impurities in brine using inductively coupled plasma atomic emission spectrography with end-on viewing of the ICP and a medium-size spectrograph, Spectrochim. Acta Part B 42 (1987) 853–858.

[19] C. Apel, D. Duchane, B. Palmer, T. Bieniewski, J. Pena, L. Cox, D. Gallimore, D.K. Vincent, M. Lopez, J. Kline, D. Steinhaus, Abstract 51. Winter Conference on Developments in Atomic Plasma Spectrochemical Analysis, San Juan, Puerto Rico, January 1980.

[20] R. Fry, T.G.H. Gower, A.R. Easgate, Axial view of an ICP emission source: It really is different inside the RF coil. Paper 284. 20th Federation of Analytical, Chemical and Spectroscopic Societies Conference (FACSS). St Louis, MO, October 1993.

[21] R.W. Foster, G. Kunselman A.E. Pallewe, Paper 582, Federation of Analytical, Chemical and Spectroscopic Societies Conference (FACSS). St Louis, MO, October 1994.

[22] H. Falk, Application of the short UV range to ICP atomic emission. Paper 88, Federation of Analytical, Chemical and Spectroscopic Societies Conference (FACSS). St Louis, MO, October 1994.

[23] A. Montaser, V.A. Fassel, Atomic emission spectrometry with a skimmed inductively coupled Ar plasma, Appl. Spectrosc. 36 (1982) 454–459.

[24] R.S. Houk, V.A. Fassel, B.R. LaFreniere, Direct detection of vacuum ultraviolet radiation through an optical sampling orifice: spatially resolved emission studies of argon resonance lines from an inductively coupled plasma, Appl. Spectrosc. 40 (1986) 94–100.

[25] B.R. LaFreniere, R.S. Houk, V.A. Fassel, Direct detection of vacuum ultraviolet radiation through an optical orifice: Analytical figures of merit for the nonmetals, metalloids, and selected metals by inductively coupled plasma atomic emission spectrometry, Anal. Chem. 59 (1987) 2276–2282.

[26] B.R. LaFreniere, R.S. Houk, D.R. Wiederin, V.A. Fassel, Direct detection of vacuum ultraviolet radiation through an optical sampling orifice: Determination of nonmetals in gaseous samples by inductively coupled plasma atomic emission spectroscopy, Anal. Chem. 60 (1988) 22–26.

[27] R.S. Houk, B.R. LaFreniere, H.B. Lim, V.A. Fassel, Extraction discharge source for enhancing analyte line intensities in inductively coupled plasma atomic emission spectrometry, Appl. Spectrosc. 41 (1987) 391–395.

[28] P.B. Farnsworth, G.M. Hieftje, Sample introduction into the inductively coupled plasma by a radiofrequency arc, Anal. Chem. 55 (1983) 1414–1417.

[29] H.B. Lim, R.S. Houk, Langmuir probe measurement of electron temperature in a supersonic jet extracted from an inductively coupled plasma, Spectrochim. Acta Part B 45 (1990) 453–461.

[30] M.W. Borer, G.M. Hieftje, Tandem sources for analytical atomic spectrometry, Spectrochim. Acta Rev. 14 (1991) 463–486.

[31] M.W. Borer, G.M. Hieftje, Design considerations for a pressure-differential tandem source for use in atomic spectrometry, J. Anal. At. Spectrom. 8 (1993) 333–338.

[32] S. Luan, H.M. Pang, R.S. Houk, Optical emission studies of the Mach disc extracted from an inductively coupled plasma with an echelle spectrometer and seg-

mented-array charge-coupled detectors, J. Anal. At. Spectrom. 11 (1996) 247–252.
[33] H. Ma'an, R.S. Houk, A secondary discharge intensifies optical emission from a Mach disk extracted from an inductively coupled plasma, J. Anal. At. Spectrom. 13 (1998) 223–228.
[34] J.C. Ivaldi, J.F. Tyson, Performance evaluation of an axially viewed horizontal inductively coupled plasma for optical emission spectrometry, Spectrochim. Acta Part B 50 (1995) 1207–1226.
[35] C. Dubuisson, E. Poussel, J.M. Mermet, Comparison of axially and radially viewed inductively coupled plasma atomic emission spectrometry in terms of signal-to-background ratio and matrix effects, J. Anal. At. Spectrom. 12 (1997) 281–286.
[36] I.B. Brenner, A. Zander, M. Cole, A. Wiseman, Comparison of axial and radial viewed ICPs for multielement analysis — effect of Na and Ca, J. Anal. At. Spectrom. 12 (1997) 897–906.
[37] I.B. Brenner, M. Zischka, B. Maichin, G. Knapp, Ca and Na interference effects in an axially viewed ICP using low and high aerosol loading, J. Anal. At. Spectrom. 13 (1998) 1257–1264.
[38] J.L. Todoli, J.M. Mermet, Minimization of acid effects at low consumption rates in an axially viewed inductively coupled plasma atomic emission spectrometer by using micronebulizers-based sample introduction systems, J. Anal. At. Spectrom. 13 (1988) 727–734.
[39] Y. Nakamura, K. Takahashi, O. Kujirai, H. Okochi, C.W. McLeod, Evaluation of an axially and radially viewed inductively coupled plasma using an echelle spectrometer with wavelength modulation and second-derivative detection, J. Anal. At. Spectrom. 9 (1994) 751–757.
[40] C. Dubuisson, E. Poussel, J.M. Mermet, J.L. Todoli, Comparison of the effect of acetic acid with axially and radially viewed inductively coupled plasma atomic emission spectrometry, J. Anal. At. Spectrom. 13 (1998) 63.
[41] J.C. Ivaldi, J.F. Tyson, Real-time internal standardization with an axially-viewed inductively coupled plasma for optical emission spectrometry, Spectrochim. Acta Part B 51 (1996) 1443–1450.
[42] C. Dubuisson, E. Poussel, J.M. Mermet, Comparison of ionic lines-based internal standardization with axially and radially viewed inductively coupled plasma atomic emission spectrometry to compensate for sodium effects on accuracy, J. Anal. At. Spectrom. 13 (1998) 1265–1269.
[43] J.M. Mermet, Revisitation of the matrix effects in inductively coupled plasma atomic emission spectrometry: the key role of the spray chamber, J. Anal. At. Spectrom. 13 (1998) 419–422.
[44] I.B. Brenner, A. Le Marchand, C. Daraed, L. Chauvet, Compensation of Ca and Na interference effects in axially and radially viewed ICPs, Microchem. J. 63 (1999) 344–353.
[45] Y. Nakamura, K. Takahashi, R. Hasegawa, Improvement of sensitivity in an axial viewed horizontal ICP-AES using of an extended torch (Japanese), Bunseki Kagaku 45/11 (1996) 1005.
[46] R.L. Dahlquist, R. Eldridge, D. Tasker, R.C. Fry, A new high electron number density (end-on) ICP. Abstract Pittsburgh Conf., Chicago, IL, 1991, p. 10.
[47] X. Huang, D. Mo, K.S. Yeah, J.D. Winefordner, Effect of radiofrequency power on laser induced fluorescence and emission spectrometry with an extended-sleeve inductively-coupled plasma torch, Anal. Chim. Acta 184 (1986) 299–306.
[48] C. Dubuisson, E. Poussel, J.L. Todoli, J.M. Mermet, Effect of sodium during the aerosol transport and filtering in inductively coupled plasma atomic emission spectrometry, Spectrochim. Acta Part B 53 (1998) 593–600.
[49] J.M. Mermet, Ionic to atomic line intensity and residence time in inductively coupled plasma-atomic emission spectrometry, Spectrochim. Acta Part B 44 (1989) 1109–1116.
[50] J.M. Mermet, Use of magnesium as a test element for inductively coupled plasma atomic emission spectrometry diagnostics, Anal. Chim. Acta 250 (1991) 85.
[51] T.S. Conver, J. Yang, J.A. Koropchak, G. Shkolnik, C. Flajnik-Rivera, Fused-silica-aperture thermospray sample introduction into axially viewed inductively coupled plasma-atomic emission spectrometry, Appl. Spectrosc. 51/1 (1997) 68–73.
[52] Y. Oomori, M. Hikawa, T. Masuda, Performance evaluation of an axially viewed inductively coupled plasma emission spectrometer. ICP Inf. Newsl. 24 (1998) 117. 7 Beijing Conference and Exhibition on Instrumental Analysis, October 1997, Shanghai, China.
[53] S.R. Koirtyhann, J.S. Jones, C.P. Jester, D.A. Yates, Use of spatial emission profiles and a nomenclature system as aids in interpreting matrix effects in the low-power argon inductively coupled plasma, Spectrochim. Acta Part B 36 (1981) 49–59.
[54] D.J. Douglas, J.B. French, An improved interface for inductively coupled plasma-mass spectrometry, Spectrochim. Acta Part B 41 (1986) 197–204.
[55] A.L. Gray, R.S. Houk, J.G. Williams, Langmuir probe potential measurements in the plasma and their correlation with mass spectral characteristics in inductively coupled plasma-mass spectrometry, J. Anal. At. Spectrom. 2 (1987) 13–20.
[56] M. Thompson, J.N. Walsh, Handbook of Inductively Coupled Plasma Spectrometry, 2nd ed, Blackie, 1989.
[57] A. Montaser, D.W. Golightly (Eds.), Inductively Coupled Plasmas in Analytical Atomic Spectrometry, 2nd ed., VCH Publishers, NY, 1992, pp. 299–339.
[58] P.W.J.M. Boumans, Inductively Coupled Plasma Emission Spectrometry, Part 1, John Wiley, New York, 1987, pp. 296–357.
[59] J.V. Sweedler, R.D. Jalkian, R.S. Pomeroy, M.B. Denton, A comparison of CCD and CID detection for

atomic emission spectroscopy, Spectrochim. Acta Part B 44 (1989) 683–692.

[60] M.J. Pilon, M.B. Denton, R.G. Schleicher, P.M. Moran, S.B. Smith, Evaluation of a new array detector atomic emission spectrometer for inductively coupled plasma atomic emission spectroscopy, Appl. Spectrosc. 44 (1990) 1613–1620.

[61] J.D. Kolczynski, D.A. Radspinner, R.S. Pomeroy, M.E. Baker, J.A. Norrwas, M.B. Denton, R.W. Foster, R.G. Schleicher, P.M. Moran, M.J. Pilon, Atomic emission spectrometry using a charge injection device (CID) detector. Internat. Lab. (1991) 49–56.

[62] T.W. Barnard, M.I. Crockett, J.C. Ivaldi, P.L. Lundberg, Design and evaluation of an echelle grating optical system for ICP-OES, Anal. Chem. 65 (1993) 1225–1230.

[63] T. Barnard, M.I. Crockett, J.C. Ivaldi, P.L. Lundberg, D.A. Yates, P.A. Levine, D.J. Sauer, Solid state detector for ICP-AES, Anal. Chem. 65 (1993) 1231–1239.

[64] A.T. Zander, R.-L. Chien, C.B. Cooper III, P.V. Wilson, An image-mapped detector for simultaneous ICP-AES, Anal. Chem. 72 (1999) 3332–3340.

[65] A.T. Zander, C.B. Cooper, R.L. Chien, US patent 5596407, 21 Jan 1997. Optical detector for echelle spectrometer.

[66] G. Thiel, K. Danzer, Direct analysis of mineral components in wine by inductively coupled plasma optical emission spectrometry (ICP-AES), Fresenius J. Anal. Chem. 357 (1997) 553–557.

[67] E. Poussel, J.M. Mermet, O. Samuel, Simple experiments for the control, the evaluation and the diagnosis of inductively coupled plasma sequential systems, Spectrochim. Acta Part B 48 (1993) 743–755.

[68] M. Carre, E. Poussel, J.M. Mermet, Drift diagnostics in inductively coupled plasma atomic emission spectrometry, J. Anal. At. Spectrom. 7 (1992) 791–797.

[69] X. Romero, E. Poussel, J.M. Mermet, The effect of sodium on analyte ionic line intensities in inductively coupled plasma atomic emission spectrometry: influence of the operating conditions, Spectrochim. Acta Part B 52 (1997) 495–502.

[70] I. Novotny, J.C. Farinas, W. Jia-liang, E. Poussel, J.M. Mermet, Effect of power and carrier gas flow rate on the tolerance to water loading in inductively coupled plasma atomic emission spectrometry, Spectrochim. Acta Part B 51 (1996) 1517–1526.

[71] J.M. Mermet, J.C. Ivaldi, Real-time internal standardization for inductively coupled plasma atomic emission spectrometry using a custom segmented-array charge coupled device detector, J. Anal. At. Spectrom. 8 (1993) 795–801.

[72] G.N. Coleman, G.H. Gower, C.J. Harris, M. O'Boyle, Optimization of Operating Conditions for an Axial-viewed ICP Torch. 37th Rocky Mountain Conference, 1995, p. 5.

[73] F. Aeschbach, Evaluation eines elektronendiffusion modellen zur berechnung von nicht Gleiwichts — elektronnenkonzentration im induktiv gekoppelten argonplasma fur die spektrochemische analyse, Spectrochim. Acta Part B 37 (1982) 987–998.

[74] L. De Galan, Some considerations on the excitation mechanism in the inductively coupled plasma, Spectrochim. Acta Part B 39 (1984) 537–550.

[75] D.C. Gregoire, The effect of easily ionizable concomitant elements on non-spectroscopic interferences in inductively coupled plasma-mass spectrometry, Spectrochim. Acta Part B 42 (1987) 895–907.

[76] M. Miller, Basic concepts in atomic emission spectroscopy, in: A. Montaser, D.W. Golightly (Eds.), Inductively Coupled Plasmas in Analytical Atomic Spectrometry, 2nd ed, VCH Publishers, New York, 1992.

[77] U. Greb, S. Leitken, written comm. Spectro, Kleve, Germany, 1998.

[78] J.W. Cooper, Plasmachem. List server. (Analytical Chemistry using ICPs, DCP's, MIP's' < PLASMACHEM-L@LISTSERV.SYR.EDU >), 1998.

[79] JY 238 brochure and data sheets, Jobin Yvon-Horiba, Longjumeau, France.

[80] J.W. Olesik, J.A. Kinzer, B. Harkleroad, Inductively coupled plasma optical emission spectrometry using nebulizers with widely different sample consumptions, Anal. Chem. 66 (1994) 2022–2030.

[81] Y. Tang, C. Trassy, Inductively coupled plasma: the role of water in axial excitation, Spectrochim. Acta Part B 41 (1986) 143–150.

[82] J.L. Todoli, J.M. Mermet, A. Canals, V. Hernandis, Acid effects in inductively coupled plasma atomic emission spectrometry with different nebulizers operated at very low sample consumption rates, J. Anal. At. Spectrom. 13 (1998) 55–62.

[83] M. Duffy, M.R. Thomas, Benefits of a dual-view ICP OES for the determination of boron, phosphorus, and sulfur in low alloy steels, At. Spectrosc. 17/3 (1996) 128–132.

[84] Liberty Series II brochure, Varian OSI, Melbourne, Australia.

[85] Varian spring seminar series, 1995. Varian OSI, Woodale, IL, USA.

[86] Varian spring seminar series and Vista CCD brochures, 1998, Varian OSI, Woodale, IL, USA.

[87] Optima 3000 XL brochure, Perkin Elmer. Wilton, Conn. USA.

[88] Panorama spectrometer brochure and data sheets, Jobin Yvon-Horiba, Longjumeau, France.

[89] End On Plasma (EOP) brochure and data sheets, Spectra, Kleve, Germany.

[90] TJA 61 E data sheet. Thermo Instruments, Mass., USA.

[91] C. Dubuisson, E. Poussel, J.M. Mermet. LODs. Written communication, 1998.

[92] R.K. Winge, V.A. Fassel, V.J. Peterson, M.A. Floyd. Inductively Coupled Plasma Atomic Emission Spec-

trometry. An Atlas of Spectral Information. Elsevier, Amsterdam, 1985.

[93] I.B. Brenner, S. Erlich, Compensation of physical and EIE effects due to high concentrations of Ca, Mg, Na, and Li for ultrasonic nebulization. Professor Peter Keliher Memorial Symposium. Abstract no. 16, p. 55. 19th Annual Meeting of the Federation of Analytical Chemistry and Spectroscopy Societies. Philadelphia, USA; ICP Newslett. 18 (1992) 481.

[94] M. De Wit, R. Blust, Determination of metals in saline and biological matrices by axial inductively coupled plasma atomic emission spectrometry using microconcentric nebulization, J. Anal. At. Spectrom. 13 (1998) 515–520.

[95] J.A. Borowiec, A.W. Boorn, M.S. Pillard, R.F. Cresser, Interference effects from aerosol ionic redistribution in analytical atomic spectrometry, Anal. Chem. 52 (1980) 1054–1059.

[96] J. Farino, J.R. Miller, D.D. Smith, R.F. Browner, Influence of solution uptake on signals and interferences in inductively coupled plasma optical emission spectrometry, Anal. Chem. 59 (1987) 2303–2309.

[97] S. Greenfield, H. McD. McGeachin, P.B. Smith, Nebulization effects with acid solutions in ICP spectrometry, Anal. Chim. Acta 84 (1976) 67–78.

[98] M. Marichy, M. Mermet, J.M. Mermet, Some effects of low acid concentrations in inductively coupled plasma atomic emission spectrometry, Spectrochim. Acta Part B 45 (1990) 1195–1201.

[99] I.B. Brenner, J.M. Mermet, I. Segal, G.L. Long, Effect of nitric and hydrochloric acids on rare earth element (REE) intensities in ICP-AES, Spectrochim. Acta Part B 50 (1995) 333–340.

[100] I.B. Brenner, I. Segal, M. Mermet, J.M. Mermet, Study of the depressive effects of nitric acid on the line intensities of rare earth elements in inductively coupled plasma atomic emission spectrometry, Spectrochim. Acta Part B 50 (1995) 333–340.

[101] F.J.M.J. Maessen, J. Balke, J.L.M. de Boer, Preservation of accuracy and precision in the analytical practice of low pressure inductively coupled plasma-atomic emission spectrometry, Spectrochim. Acta Part B 37 (1982) 517–526.

[102] I.I. Stewart, J.W. Olesik, The effect of nitric acid concentration and nebulizer gas flow rates on aerosol properties and transport rates in inductively coupled plasma sample introduction, J. Anal. At. Spectrom. 13 (1998) 1249–1256.

[103] J.W. Milburn, Automated addition of internal standards for axial-view plasma ICP spectrometry using the Optima 3000 XL, At. Spectrosc. 17 (1996) 9–14.

[104] M. Thompson, M.H. Ramsey, Matrix effects due to calcium in inductively coupled plasma-atomic emission from spectrometry, Analyst 110 (1985) 1413–1422.

[105] M.H. Ramsey, M. Thompson, A predictive model of plasma matrix effects in inductively coupled plasma atomic emission spectrometry, J. Anal. At. Spectrom. 1 (1986) 185–193.

[106] M.W. Blades, G. Horlick, Interference from easily ionizable element matrices in inductively coupled plasma emission spectrometry — a spatial study, Spectrochim. Acta Part B 36 (1981) 881–900.

[107] J. Davies, R.D. Snook, Spatial emission characteristics and excitation mechanisms in the inductively coupled plasma, J. Anal. At. Spectrom. 1 (1986) 325–330.

[108] M.R. Tripkovic, I.D. Holclajtner-Autonovic, Sudy of the matrix effects of easily and non-easily ionizable elements in an inductively coupled argon plasma, J. Anal. At. Spectrom. 8 (1993) 349–357.

[109] P.J. Galley, G.M. Hieftje, Easily ionized element (EIE) interferences in inductively coupled plasma atomic emission spectrometry — II. Minimization of EIE effects by choice of observation zone, Spectrochim. Acta Part B 49 (1994) 703–724.

[110] J.W. Olesik, L.J. Smith, E.J. Williamsen, Signal fluctuations due to individual droplets in inductively coupled plasma atomic emission spectrometry, Anal. Chem. 61 (1989) 2002–2008.

[111] D.E. Nixon, Excitation modulation by water: Effects of desolvation on line intensities, temperatures, and ion–atom ratios produced by inductively coupled plasmas, J. Anal. At. Spectrom. 5 (1990) 531–536.

[112] K. O'Hanlon, L. Ebdon, M. Foulkes, Effect of easily ionizable elements on solutions and slurries in an axially viewed inductively coupled plasma, J. Anal. At. Spectrom. 11 (1996) 427–436.

[113] R.M. Belchamber, G. Horlick, Correlation study of internal standardization in inductively coupled plasma atomic emission spectrometry, Spectrochim. Acta Part B 37 (1982) 1037–1046.

[114] W.B. Barnett, V.A. Fassel, R.N. Kniseley, An experimental study of internal standardization in analytical atomic emission spectroscopy, Spectrochim. Acta Part B 26 (1970) 139–161.

[115] A.E. Watson, G.M. Russell, Use of a high power ICP source and spectrometer in general metallurgical analysis, ICP Inf. Newsl. 4 (1979) 441–457.

[116] J.R. Sedcole, J. Lee, M.W. Pritchard, Internal standard selection in the presence of matrix interactions in an inductively coupled argon plasma optimized for simultaneous multi-element analysis by atomic emission spectrometry, Spectrochim. Acta Part B 41 (1986) 227–235.

[117] S.A. Myers, D.H. Tracy, Improved performance using internal standardization in inductively coupled plasma emission spectroscopy, Spectrochim. Act Part B 38 (1983) 1227–1253.

[118] I.B. Brenner, A.E. Watson, G.M. Russell, M. Goncalves, A new approach to the determination of the major and minor elements in silicate and phosphate rocks, Chem. Geol. 28 (1980) 321–330.

[119] X. Romero, E. Poussel, J.M. Mermet, Influence of the operating conditions on the efficiency of internal stan-

dardization in inductively coupled plasma atomic emission spectrometry, Spectrochim. Acta Part B 52 (1997) 487–493.

[120] M.H. Ramsey, M.J. Thompson, High-accuracy analysis by inductively coupled plasma atomic emission spectrometry using the parameter related internal standard method, J. Anal. At. Spectrom. 2 (1987) 497–502.

[121] J.L.M. de Boer, M. Velterop, Empirical procedure for the reduction of mixed-matrix effects in inductively coupled plasma atomic-emission spectrometry using an internal standard and proportional correction, Fresenius J. Anal. Chem. 356 (1996) 362–370.

[122] J.L.M. de Boer, W. van Leewen, U. Kohlmeyer, P.M. Breugen, The determination of chromium, copper, and nickel in groundwater using axial plasma inductively coupled plasma atomic emission spectrometry and proportional correction matrix effect reduction, Fresenius J. Anal. Chem. 360 (1998) 213–218.

[123] A. Lorber, Z. Goldbart, A. Harel, E. Sharvit, M. Eldan, Application of the generalized internal reference method to high accuracy assay of metallurgical samples by ICP, Spectrochim. Acta Part B 41 (1986) 105–113.

[124] A. Lorber, Z. Goldbart, Application of the generalized internal reference method for the characterization of parameters causing drift in inductively coupled plasma emission spectrometry, Anal. Chim. Acta 161 (1984) 163–173.

[125] I. Jarvis, K.E. Jarvis, Plasma spectrometry in the earth sciences, Chem. Geol. 95 (1992) 1–191.

[126] R.I. Botto, Multielement analysis of fossil fuels and related materials by ICP-AES, Spectrochim. Acta Rev. 14 (1991) 141–159.

[127] I.B. Brenner, A. Zander, Evaluation of a ultrasonic nebulizer–membrane separation interface (USN-MEMSEP) with ICP-AES for determination of trace elements by solvent extraction, Fresenius J. Anal. Chem. 355 (1996) 559–570.

[128] K. Govindaraju, Compilation of working values and sample description for 383 geostandards, Geostands. Newsl. 18 (1994) (1994) 158.

[129] W.M. Johnson, J.A. Maxwell, Rock and Mineral Analysis, 2nd ed, John Wiley, NY, 1981, p. 489.

[130] I.B. Brenner, S. Vats, A.T. Zander, A new CCD axially viewed ICP atomic emission spectrometer for simultaneous multi-element geoanalysis — determination of the major and minor elements in silicate rocks, J. Anal. At. Spectrom. 14 (1999) 1231–1237.

[131] K.P. Raven, J.W. Reynolds, R.H. Loeppert, Trace-element analyses of fertilizers and soil amendments by axial-view inductively coupled plasma atomic-emission spectrophotometry, Comm. Soil Sci. Plant Anal. 28/3-5 (1997) 237–257.

[132] K.W. Barnes, Trace metal determinations in fruit, juice, and juice products using an axially viewed plasma, At. Spectrosc. 18 (1997) 84.

[133] K.W. Barnes, A streamlined approach to the determination of trace elements in foods, At. Spectrosc. 19 (1998) 31.

[134] A. Ryan. Direct analysis of milk powder on the Liberty Series II ICP-AES with the axially viewed plasma. ICP-AES Instruments at Work, ICP-21, Varian Associates, August 1997, p. 7.

[135] K.D. Besecker, C.B. Rhoades, B.T. Jones, K.W. Barnes, At. Spectrosc. 19 (1998) 48.

[136] K.D. Besecker, C.B. Rhoades, B.T. Jones, K.W. Barnes, Closed vessel nitric acid digestion of polymers, At. Spectrosc. 19 (1998) 55.

[137] M.D. Seltzer, Instrumental considerations for high-sensitivity continuous emissions monitoring of hazardous air pollution metals, Process Control Qual. 7/2 (1995) 71–77.

[138] T. Kato, T. Uehiro, A. Yasuhara, M. Morita, Determination of methylmercury species by capillary column gas chromatography with axially viewed inductively coupled plasma atomic emission spectrometric detection, J. Anal. At. Spectrom. 7 (1992) 15–18.

[139] R.H. Wendt, V.A. Fassel, Anal. Chem. 38 (1966) 337.

[140] S. Greenfield, P.B. Smith, A.E. Breeze, N.M.D. Chilton, Anal. Chim. Acta 41 (1968) 385.

[141] W.B. Barnett, V.A. Fassel, R.N. Kniseley, Theoretical principles of internal standardization in analytical emission spectroscopy, Spectrochim. Acta Part B 23 (1968) 643–664.

[142] G.D. Rayson, Inductively coupled plasma axial viewing absorption technique with linear-flow coolant gas, Spectrochim. Acta Part B 46 (1991) 1237–1242.

[143] G.D. Rayson, D.Y. Shen, Application of an inductively coupled argon plasma axial viewing absorption technique using a power modulated plasma, Spectrochim. Acta Part B 47 (1992) 553.

[144] G.D. Rayson, D.Y. Shen, Inductively coupled plasma axial viewing absorption technique, Anal. Chem. 62 (1990) 1239–1241.

[145] G.D. Rayson, D.Y. Shen, Impact of scattering on axial-viewing absorption measurements within an inductively coupled plasma, Appl. Spectrosc. 45 (1991) 706–708.

[146] D.Y. Shen, Development of an Inductively Coupled Argon Plasma Axial Viewing Atomic Absorption Technique. New Mexico State University Institution Code-0143. Ph.D. Thesis, 1991.

[147] S.A. Darke, J.F. Tyson, Review of solid sample introduction for plasma spectrometry and a comparison of results for laser ablation, electrothermal vaporization and slurry nebulization, Microchem. J. 50 (1994) 310–336.

[148] C.W. McLoed, M.W. Routh, M.W. Tikkanen. Introduction of solids into plasmas, ch. 16, in: A. Montaser, D.W. Golightly (Eds.), Inductively Coupled Plasmas in Analytical Spectrometry, 2nd ed. VCH Publishers, New York, pp 721–780.

[149] A.A. Verbeek, I.B. Brenner, Slurry nebulization of geological materials into argon, argon–nitrogen, and

argon oxygen inductively coupled plasmas, J. Anal. At. Spectrom. 4 (1989) 23–26.
[150] G.L. Long, I.B. Brenner, Analysis of ceramic, geological and related refractory materials by slurry injection mixed gas inductively coupled plasma atomic emission spectrometry, J. Anal. At. Spectrom. 5 (1990) 495.
[151] L. Halicz, I.B. Brenner, O. Yoffe, Direct solids analysis of geological samples using slurry nebulization inductively coupled plasma atomic emission spectrometry, J. Anal At. Spectrom. 4 (1993) 475–480.
[152] K.E. Jarvis, J.G. Williams, The analysis of geological samples by slurry nebulization inductively coupled plasma-mass spectrometry (ICP-MS), Chem. Geol. 77 (1989) 53–63.
[153] I.B. Brenner, A. Zander, S. Kim, A. Henderson, Direct solids analysis of geological and nonconducting materials using spark ablation and slurry nebulization, Spectrosc. Eur. 7/4 (1995) 24–32.
[154] I.B. Brenner, A. Zander, Sequential multi-element analysis of coals by slurry nebulization Ar, Ar–O_2 and N_2 inductively coupled plasma atomic emission spectrometry, Spectroscopy 13 (1998) 14.
[155] L. Ebdon, M. Foulkes, K. O'Hanlon, Slurry nebulization in plasmas, J. Anal At. Spectrom. 12 (1997) 213–229.
[156] I.B. Brenner, A. Zander. Application of an axially viewed ICP and slurry nebulization for sequential multielement analysis of geological materials. ICP Inf. Newsl. (submitted).
[157] A. Aziz, J.A.C. Broekaert, K. Laqua, F. Leis, A study of direct analysis of solid samples using spark ablation combined with excitation in an inductively coupled plasma, Spectrochim. Acta Part B 39 (1984) 1091–1103.
[158] C. Webb, C.B. Cooper, A.T. Zander, J.T. Arnold, E.S. Lile, Direct solid sampling for analysis with inductively coupled plasma using a novel electronic spark source, J. Anal. At. Spectrom. 9 (1994) 263–266.
[159] I.B. Brenner, A. Zander, S. Kim, C. Holloway, Multielement analysis of geological and related non-conducting materials using spark ablation and a sequential spectrometer", Spectrochim. Acta Part B 50 (1995) 562–582.
[160] M. Gagean, J.M. Mermet, Comparison of ultraviolet laser ablation and spark ablation of metals and alloys for analysis by axially viewed inductively coupled plasma atomic emission spectrometry, J. Anal. At. Spectrom. 12 (1997) 189–193.
[161] I.B. Brenner, A.T. Zander. Multielement analysis of silicate rocks using spark ablation and an axially viewed ICP multichannel CCD spectrometer Fresenius J. Anal. Chem. (submitted).
[162] L. Moenke-Blankenberg, Laser ICP-spectrometry, Spectrochim. Acta Rev. 15 (1993) 1–37.
[163] L. Moenke-Blankenberg, Laser Micro Analysis, Wiley Interscience, New York, NY, 1989, p. 288.
[164] S.A. Darke, J.F. Tyson, Interaction of laser radiation with solid materials and its significance to analytical spectrometry—a review, J. Anal. At. Spectrom. 8 (1993) 145–209.
[165] P.M. Outridge, W. Doherty, D.C. Gregoire, The formation of trace element-enriched particulates during laser ablation of refractory materials, Spectrochim. Acta Part B 51 (1996) 1451–1462.
[166] M. Hemmerlin, J.M. Mermet, M. Bertucci, P. Zydowicz, Determination of additives in PVC materials by UV laser ablation inductively coupled plasma atomic emission spectrometry, Spectrochim. Acta Part B 52 (1997) 421–430.
[167] V. Karanosios, G. Horlick, A computer controlled direct sample insertion device for inductively coupled plasma-atomic emission spectrometry, Spectrochim. Acta Part B 45 (1990) 85–104.
[168] C.D. Skinner, E.D. Salin, Axial viewing and modified cup design for direct sample insertion inductively coupled plasma atomic emission spectrometry, J. Anal. At. Spectrom. 12 (1997) 725–732.
[169] J. Hassler, O. Förster, A. Detcheva, P. Perzl, K. Florian, Working with a new ETV device and an ICP-CID spectrometer. 8th International Colloquium on Solid Sampling with Atomic Spectrometry, Budapest, Hungary, ICP Inf. Newsl. 24 (1998) 444.
[170] W. Schrön, A. Liebmann, G. Nimmerfall, Solid sample analysis in sediments, soils and rocks by ETV-ICP-OES and GF-AAS. 8th International Colloquium on Solid Sampling with Atomic Spectrometry, Budapest, Hungary, ICP Inf. Newsl. 24 (1998) 448.
[171] R.K. Winge, J.S. Crain, R.S. Houk, High-speed photographic study of plasma fluctuations and intact aerosol particles or droplets in inductively coupled plasma-mass spectrometry, J. Anal. At. Spectrom. 6 (1991) 601–604.
[172] J.W. Olesik, J.C. Fister III, Incompletely desolvated droplets in argon inductively coupled plasmas: their number, original size and effect on emission intensities, Spectrochim. Acta Part B 46 (1991) 851–868.